GIA® NEWS FROM RESEARCH

The report indicates the status of a research project that is still ongoing within GIA.
Comments on this and other reports and their direction are warmly welcomed as are offers of collaboration.
Contact information can be found in the "about the authors" section on page 34.

Update on "low-temperature" heat treatment of Mozambican ruby: A focus on inclusions and FTIR spectroscopy

Sudarat Saeseaw, Boodsakorn Kongsomart, Ungkhana Atikarnsakul, Charuwan Khowpong, Wim Vertriest and Wasura Soonthorntantikul

April 25, 2018

Mozambican ruby with spotted platelets that indicate heat treatment. Fiber-optic illumination. FOV 1.0 mm. Photo: C. Khowpong © GIA.

Table of Contents

Introduction

Gemstones have been treated for as long as they have been used by humans. The supply of untreated high-quality gems is so incredibly small that people have always tried to find ways to optimize the other material found in the mines. Treatments come in many different forms and degrees of quality improvement. Dyeing to create color, oiling to hide fractures, heat treatment to increase clarity and optimize color, irradiation to modify color, and impregnation for better stability are just a few examples (Nassau, 1981).

In the case of corundum, heat treatment is the most common form. By applying the correct heating process, color can be introduced, strengthened, reduced, or removed. These variations are determined by an interplay between the gemstones, temperature profile during treatment, duration of heating, heating atmosphere (reducing or oxidizing), and the presence of added chemicals (Hughes, 2016; Emmett et al., 2003, 1993).

Recent developments have caused drastic changes in heat treatment applications. Since 2009, Mozambique has been an important source of rubies in the world trade. It was quickly discovered that these stones reacted well to a form of heat treatment that used lower temperatures. This modern treatment at low temperatures is distinguished from the classic high-temperature methods by comparing their effect on the minute particles in the stones. These second-phase microcrystals are most commonly rutile (Ti-oxide) that takes the form of fine clouds or silk. During low-temperature treatment, these inclusions are not dissolved in the corundum lattice. This is clearly the case for high-temperature treatment, where silk is obviously altered or even completely diffused.

Since heat treatment depends on more than the temperature alone, it is very hard to state a clear temperature boundary between low-temperature and high-temperature treatment. The most important factors to consider in this case are temperature and time. The speed of the process increases considerably with higher temperatures, but longer heating periods at lower temperatures might yield similar results. A rough guideline for the temperature boundary is somewhere between 1200 and 1350°C.

Preliminary studies on low-temperature treatment have been published (Pardieu, Saeseaw et al., 2015; Sripoonjan, Wanthanachaisaeng et al., 2016). Both of these publications mention subtle alterations, notably in stained fractures and silk platelets. Spectroscopy showed promising results, but the results were inconclusive due to the small sample sizes.

Because heat treatment processes are constantly evolving, updated data needs to be collected regularly. The objective of this project is to observe changes in Mozambican rubies during known treatment conditions (temperature and duration). The focus is on inclusions and FTIR spectra after heat treatment.

Materials and Methods

2.1 Sample Fabrication

Forty-seven (47) samples from GIA's reference collection were selected for the heat treatment experiments. All samples were collected during GIA field expedition FE 71 (August 2015), catalogued as C1 type (collected from the miner at the mine, but without witnessing the mining). The samples were mined in Mugloto, where ruby was discovered in 2011–2012.

Two samples were fabricated as optical wafers with two polished windows parallel to the optic c-axis using GIA's corundum c-axis device for sample preparation (Thomas, 2009). All samples were fabricated with at least two parallel windows. This allows platelets and other inclusions to be observed clearly.

In addition to the initial 47 stones, we studied infrared spectra from 200 samples of natural unheated Mozambique ruby.

2.2 Instrumentation

SAMPLE PHOTOGRAPHY

The true color of the 47 samples was recorded using a Canon EOS 5D camera, with a Canon Macro MP-E 65 mm lens adapted to the camera stand. This was done both before and after heat treatment. In order to produce consistent results for each sample, the photographs were taken under exactly the same lighting conditions, with the reference samples placed in a Logan Electric Tru-View 810 Color Corrected Light Box (5000 K lamp). A neutral-density filter was used to calibrate the camera light box combination to produce a neutral gray. High-resolution reference photographs were then collected using transmitted light. As the reference photographs were taken of wafers with windows cut perpendicular or parallel to the c-axis, the color of the samples in the photographs taken using transmitted light can be considered representative of the color, of a nearly pure o-ray and a mixture of o-ray and e-ray, respectively.

Photomicrographs of internal features were captured at different magnifications with Nikon SMZ 18 and Nikon SMZ 1500 systems using darkfield, brightfield, diffused, and oblique illumination, together with a fiber-optic light source when necessary. It should be noted that the microscope's magnification power was taken into consideration when calculating the field of view (FOV) information in the captions.

INFRARED ABSORPTION (FTIR) SPECTROSCOPY

Fourier-transform infrared (FTIR) spectroscopy was performed using a Thermo Nicolet 6700 FTIR spectrometer equipped with an XT-KBr beam splitter and a mercury-cadmium-telluride (MCT) detector operating with a 4x beam condenser accessory. The resolution was set at 2 cm^{-1} with 1.928 cm^{-1} data spacing. The spectra obtained were converted to an absorption coefficient using $\alpha = 2.303A/d$, where A is absorbance and d is the path length in centimeters. Each sample was scanned 200 times.

UV-VIS-NIR SPECTROSCOPY

Ultraviolet-visible-near infrared (UV-Vis-NIR) spectra were collected with a Hitachi U-2910 spectrophotometer specially modified at GIA to include a rotatable polarizer to allow the separate collection of both the ordinary (o-) and extraordinary (e-) rays. A wavelength resolution of 1.5 nm was applied. The spectra obtained were corrected by calculating the reflection loss from the refractive index data, and the data was converted to show their absorption coefficients (α, cm^{-1}) using $\alpha = 2.303\ A/d$, where *A* is absorbance and *d* is the path length in centimeters.

RAMAN SPECTROSCOPY

To identify mineral inclusions, Raman spectra were obtained using a Renishaw inVia Raman microscope fitted with a 514 nm argon-ion laser. The spectra were collected in the 100–1500 cm^{-1} range. Each spectrum was accumulated a minimum of five times until the signal-to-noise ratio was adequate. The calibration was performed using the 520.5 cm^{-1} line of a silicon wafer. In all cases, the RRUFF database was used as a reference when identifying inclusions. Spectral comparisons were performed using Renishaw Wire (version 3.4) and/or Thermo Galactic Spectra ID (version 3.02) software.

LASER ABLATION–INDUCTIVELY COUPLED PLASMA–MASS SPECTROMETRY (LA-ICP-MS)

For chemical analysis, we used LA-ICP-MS technology with a Thermo Fisher Scientific iCAP Q inductively coupled plasma–mass spectrometer coupled with a Q-switched Nd:YAG laser ablation device operating at a wavelength of 213 nm. Laser conditions employed were 55 µm diameter laser spots, a fluency of around 10 J/cm^2, and a 15 Hz repetition rate. Twelve spots were analyzed on each wafer. For the ICP-MS operations, the forward power was set at approximately 1350 W and the typical nebulizer gas flow was approximately 0.80 L/min. The carrier gas used in the laser ablation unit was He, set at about 0.50 L/min. The criteria for the alignment and tuning sequence were to maximize Be counts and keep the ThO/Th ratio below 2%. A special set of synthetic corundum reference standards was used for quantitative analysis. All elemental measurements were normalized on Al (internal element standard). This value approximates the chemical composition of corundum.

HEAT TREATMENT

Heat treatment experiments were conducted with a Thermolyne benchtop 1100°C muffle furnace, FB1400 model manufactured by Thermo Scientific (Figure 1). Samples were placed on a high-purity Al_2O_3 ceramic felt and heated in air to different temperatures and durations as follows:

i) Samples were heated at
   a. 600°C for 24 hours; *6 samples*
   b. 700°C for 8 and 24 hours; *3 and 2 samples, respectively*
   c. 800°C for 2 hours and 40 minutes, 8 hours, and 24 hours; *4, 3, and 2 samples, respectively*
   d. 900°C for 2 hours and 40 minutes and 8 hours; *2 samples each condition*

ii) Samples were heated at 800°C for 2 hours and 40 minutes three consecutive times (4 samples)

iii) Samples were heated at 800°C for 2 hours and 40 minutes (23 samples) (see Figure 1). These stones were chosen for FTIR study and separated into three groups:
   a. 10 samples exhibiting a 3309 cm^{-1} peak of medium intensity
   b. 10 samples exhibiting a 3309 cm^{-1} peak of low intensity
   c. 3 samples exhibiting boehmite/kaolinite features in their spectra

All samples were allowed to cool down to room temperature after the heating experiment was completed. Data collection (color appearance, inclusions, infrared, and UV-Vis-NIR spectra) was recorded on each sample and compared to the results obtained before heat treatment. It is important to note that each sample was studied both before and after the heat treatment experiments; the samples studied are shown in appendix A.

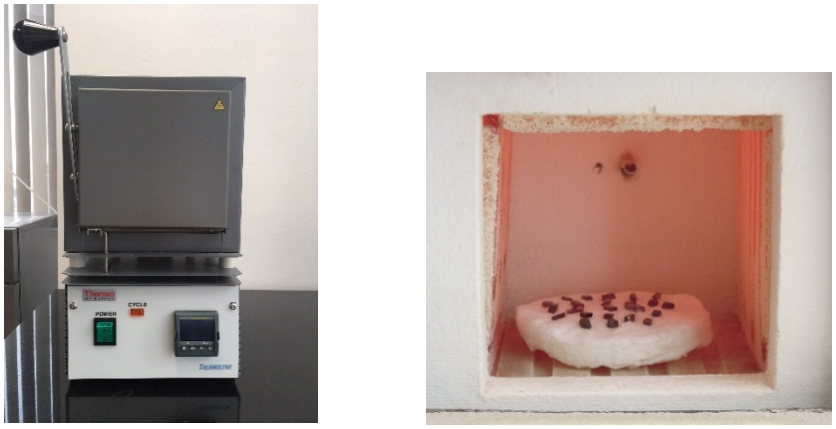

Figure 1: Left: The furnace used in GIA Bangkok for the experiments discussed in this work. Right: Some of the samples to be removed from the furnace at the end of an experiment.

Results

3.1 Effects on color appearance

Mozambique rubies often show a purplish tint, and heat treatment has been applied to reduce any blue component. In this experiment, we found that the color did not change when the stones were heated at 600°C or 700°C. They only started changing color when heated at 800°C (Figure 2). Color-calibrated images of the stones before and after heating are shown in appendix A.

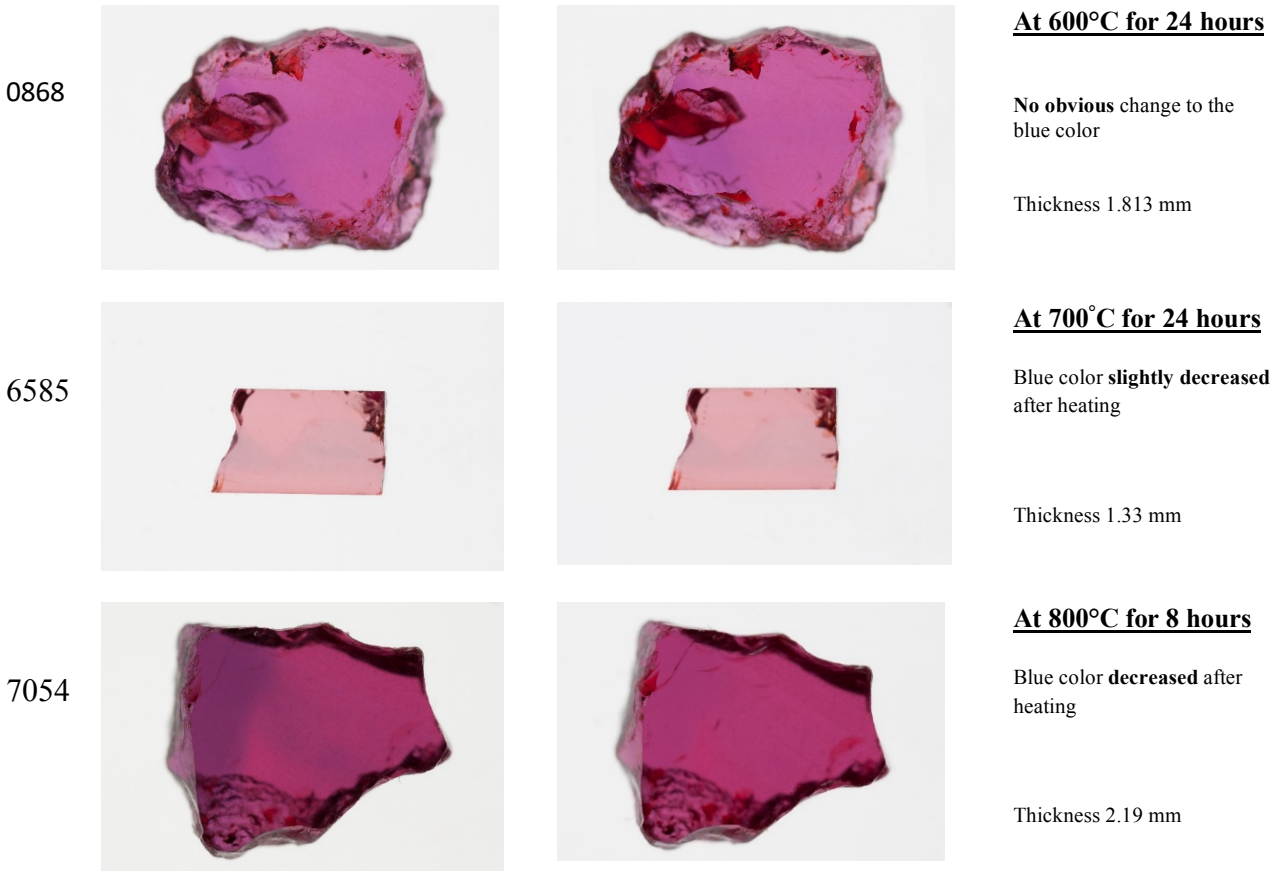

Figure 2: Color-calibrated photo after heat treatment using different heating conditions.

3.2 Effect of heat treatment on inclusions

Typical Mozambican ruby inclusions are needles, particles, platelets, and mineral inclusions such as mica, amphibole, feldspar, and chalcopyrite (Pardieu et al., 2013, 2015). Growth tubes occur along twinning planes and often contain minerals such as boehmite and kaolinite. Surface-reaching fractures contain limonite or other iron-oxide-hydroxide minerals. In this study, we focused on the changes of platelets because it is easier to spot signs of heat treatment on mineral inclusions. In our previous study, we found the platelets appeared spotted or deteriorated after heat treatment.

EFFECT ON PLATELETS

Platelets are a common inclusion seen in Mozambican rubies, although they can also be seen in rubies from other localities such as Madagascar. These platelets are in different orientations. Therefore, it is important to carefully observe these platelets under a gemological microscope, as some are affected by heat treatment and some are not. In this study, we found affected platelets in 22 out of the 47 samples. We noticed that the platelets showed no change when the stones were heated at 600°C for 24 hours, and slightly changed when heat treated at 700°C. Alteration of platelets was obvious when the stones are heated at higher temperature or for a longer duration. For example, we observed many platelets showing bright spots when heated at 700, 800, and 900°C for 24 hours, whereas only a few platelets were altered when heated for 8 hours. See Figure 3–Figure 29.

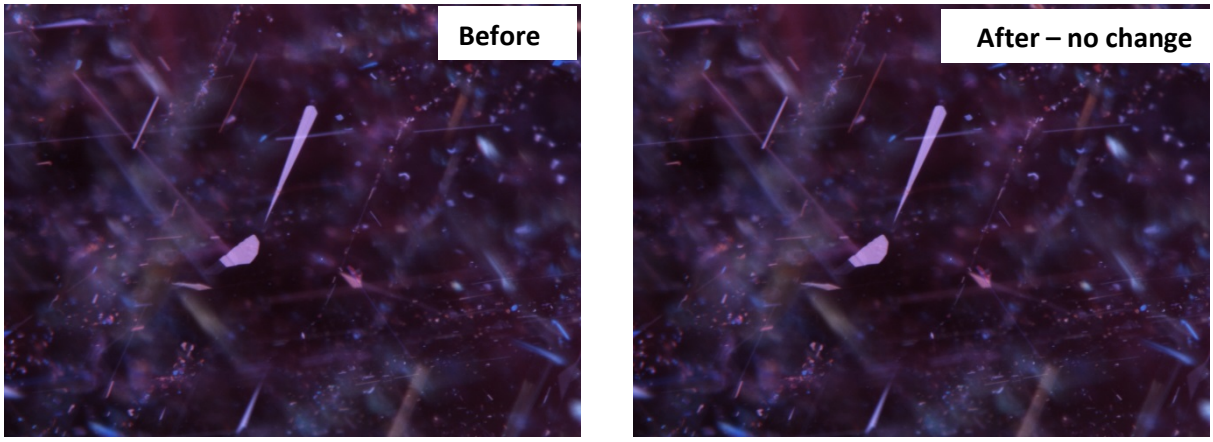

Figure 3: Samples 6566, before (left) and after (right) heat treatment at **600°C for 24 hours**. We can see reflective platelets and needles; after heat treatment there were no changes in the platelets. Fiber-optic illumination. FOV 1.0 mm. Photo: B. Kongsomart © GIA.

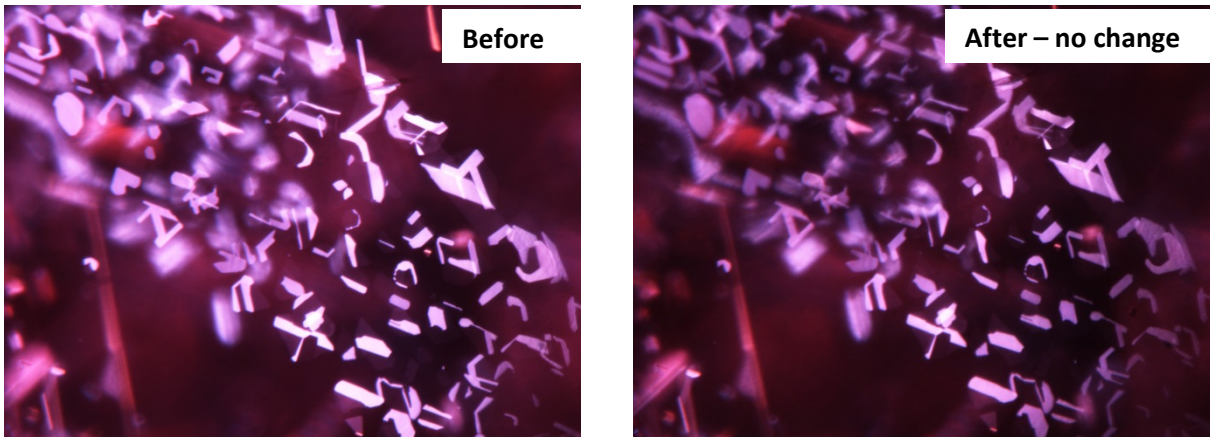

Figure 4: Sample 0868, before (left) and after (right) heat treatment at **600°C for 24 hours**. Groups of reflective platelets were not altered after heat treatment. Fiber-optic illumination. FOV 0.7 mm. Photo: B. Kongsomart © GIA.

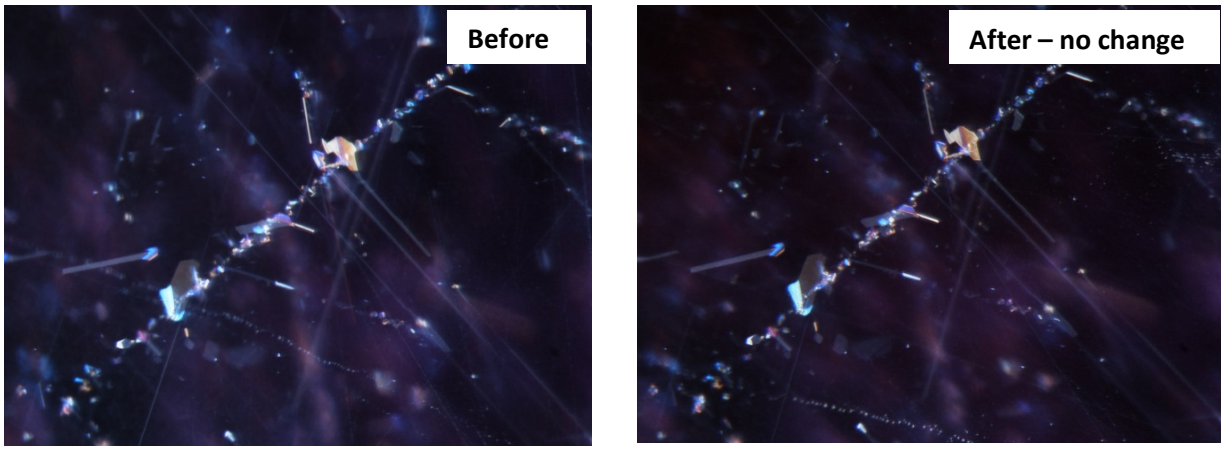

Figure 5: Sample 7008, before (left) and after (right) heat treatment at **700°C for 8 hours**. There was no change in the platelets after heat treatment. Fiber-optic illumination. FOV 0.7 mm. Photo: B. Kongsomart © GIA.

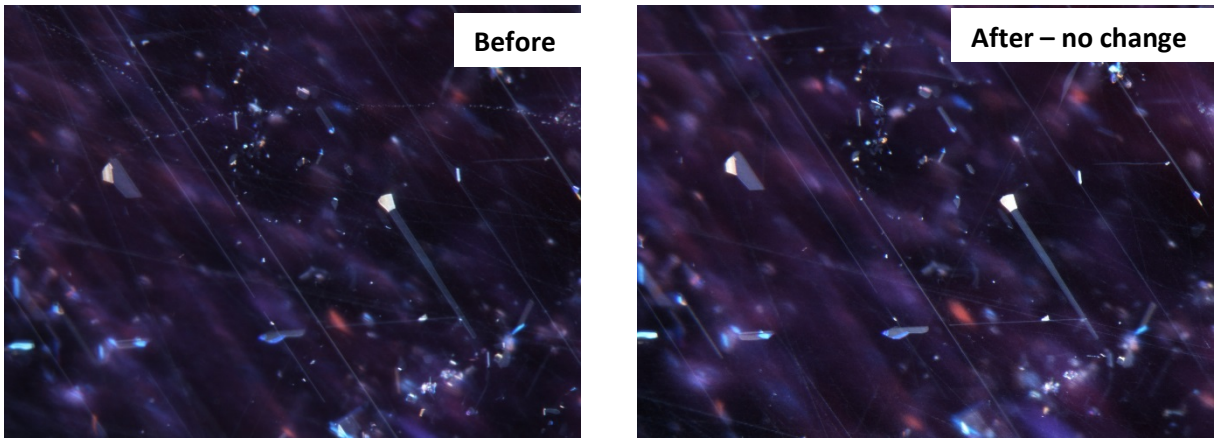

Figure 6: Sample 7008, before (left) and after (right) heat treatment at **700°C for 8 hours**. Groups of reflective platelets showed no visible change after heat treatment. Fiber-optic illumination. FOV 0.9 mm. Photo: B. Kongsomart © GIA.

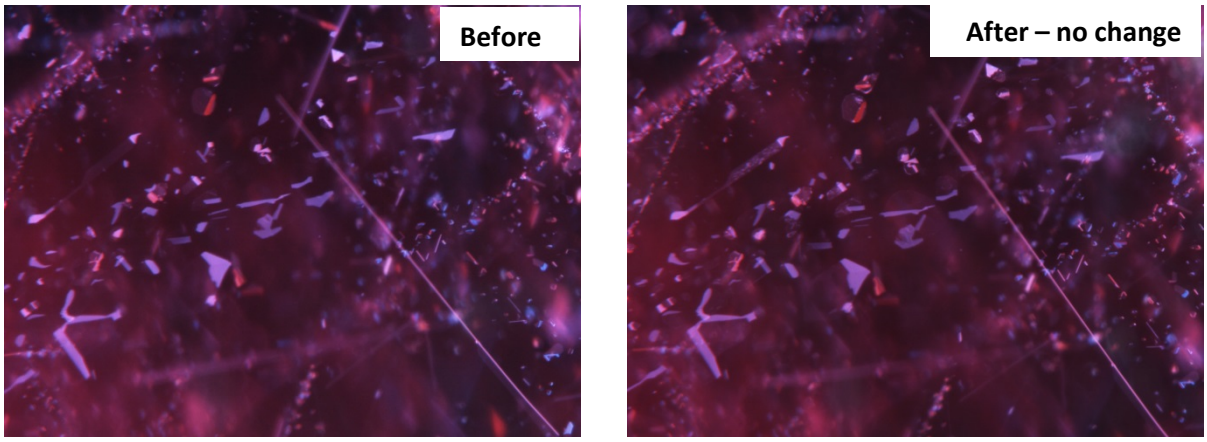

Figure 7: Sample 6570, before (left) and after (right) heat treatment at **700°C for 24 hours**. There was no visible change in the reflective platelets. Darkfield illumination. FOV 1.1 mm. Photo: B. Kongsomart © GIA.

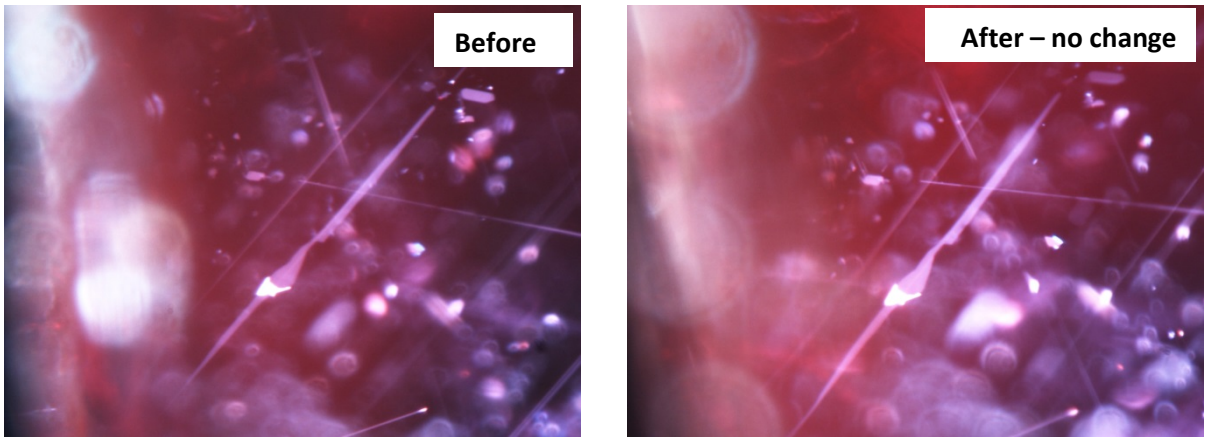

Figure 8: Sample 6585, before (left) and after (right) heat treatment at **700°C for 24 hours.** There was no visible change in the reflective platelets. Darkfield illumination. FOV 0.8 mm. Photo: B. Kongsomart © GIA.

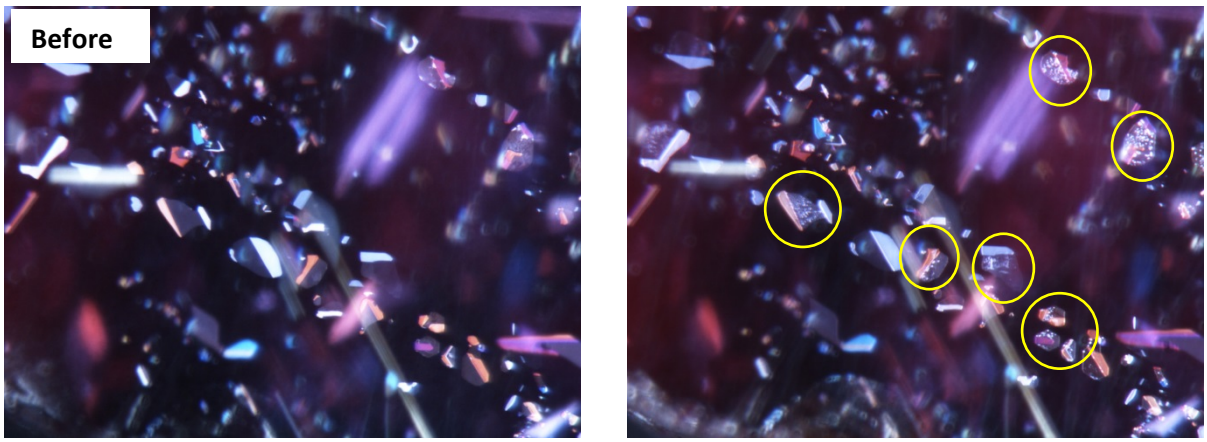

Figure 9: Sample 6570, before (left) and after (right) heat treatment at **700°C for 24 hours**. Some of the platelets showed spots after heat treatment. Fiber-optic illumination. FOV 0.7 mm. Photo: B. Kongsomart © GIA.

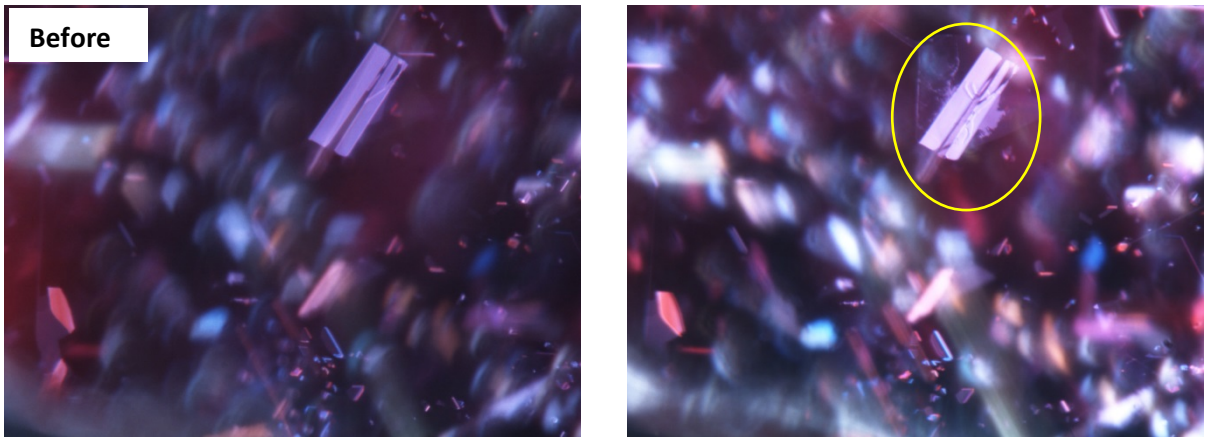

Figure 10**:** Sample 6570, before (left) and after (right) heat treatment at **700°C for 24 hours.** Platelets appeared spotty after heat treatment. Fiber-optic illumination. FOV 0.7 mm. Photo: B. Kongsomart © GIA.

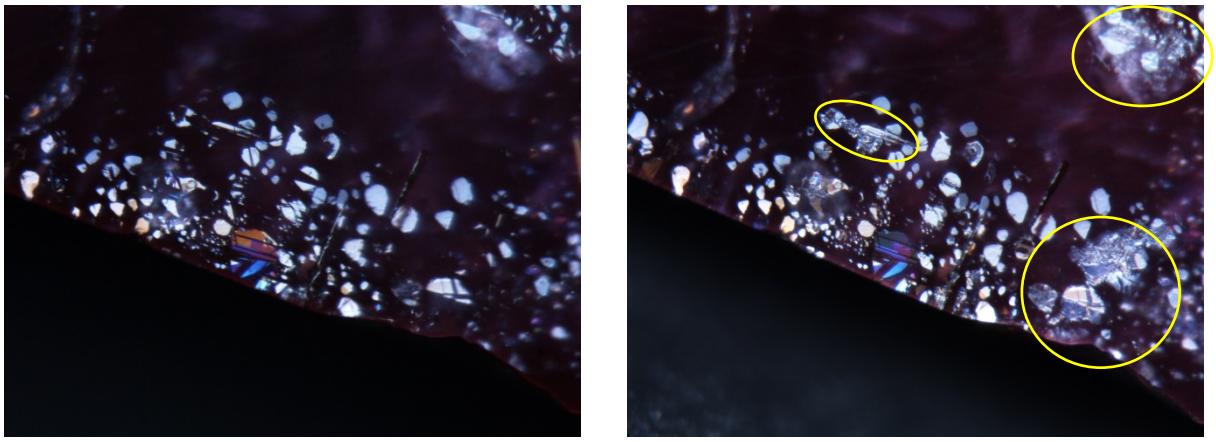

Figure 11**:** Sample 6570, before (left) and after (right) heat treatment at **700°C for 24 hours**. After heat treatment, thin films were more whitish and bright spots were created. Fiber-optic illumination. FOV 0.7 mm. Photo: B. Kongsomart © GIA.

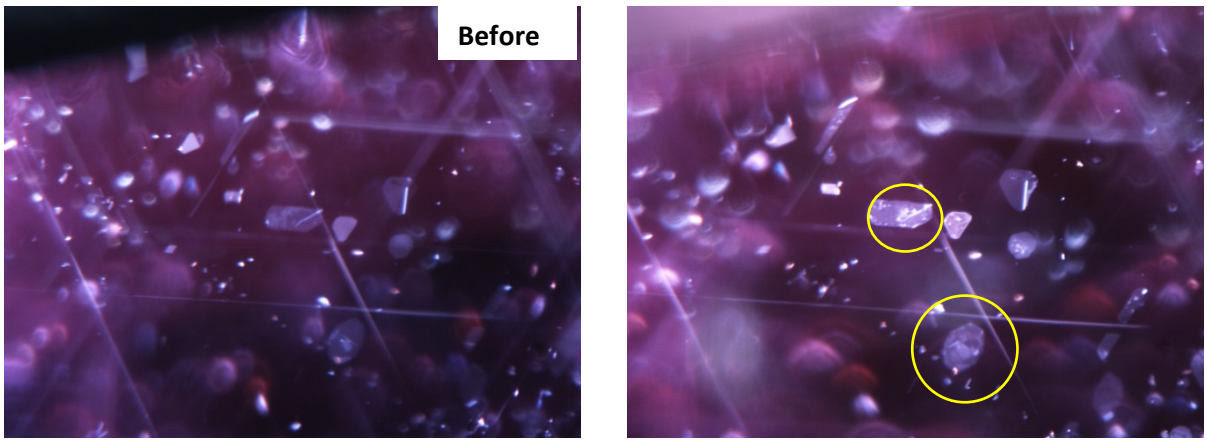

Figure 12**:** Sample 6585, before (left) and after (right) heat treatment at **700°C for 24 hours**. After heat treatment, platelets were whiter and bright spots were created. Fiber-optic illumination. FOV 0.9 mm. Photo: B. Kongsomart © GIA.

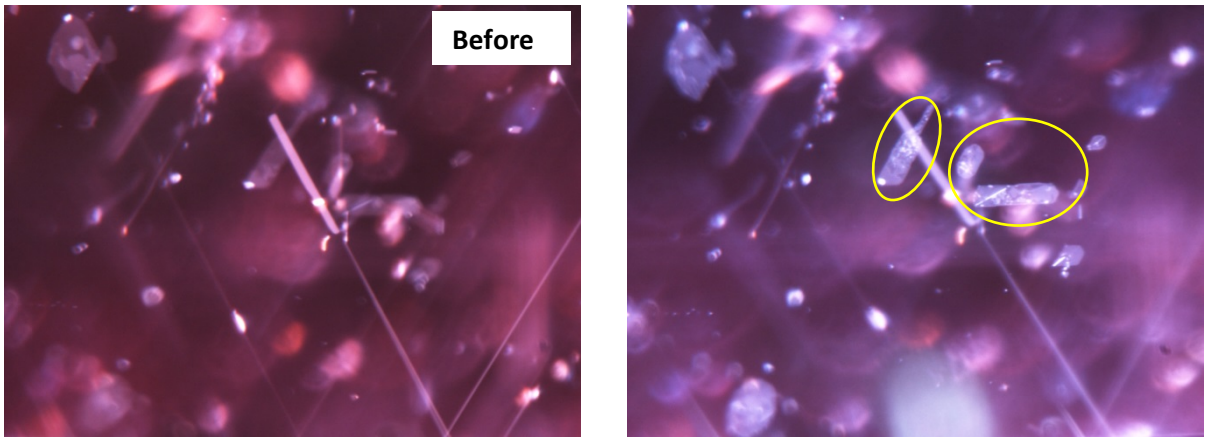

Figure 13**:** Sample 6585, before (left) and after (right) heat treatment at **700°C for 24 hours**. After heat treatment, platelets were whiter and bright spots were created. Fiber-optic illumination. FOV 0.7 mm. Photo: B. Kongsomart © GIA.

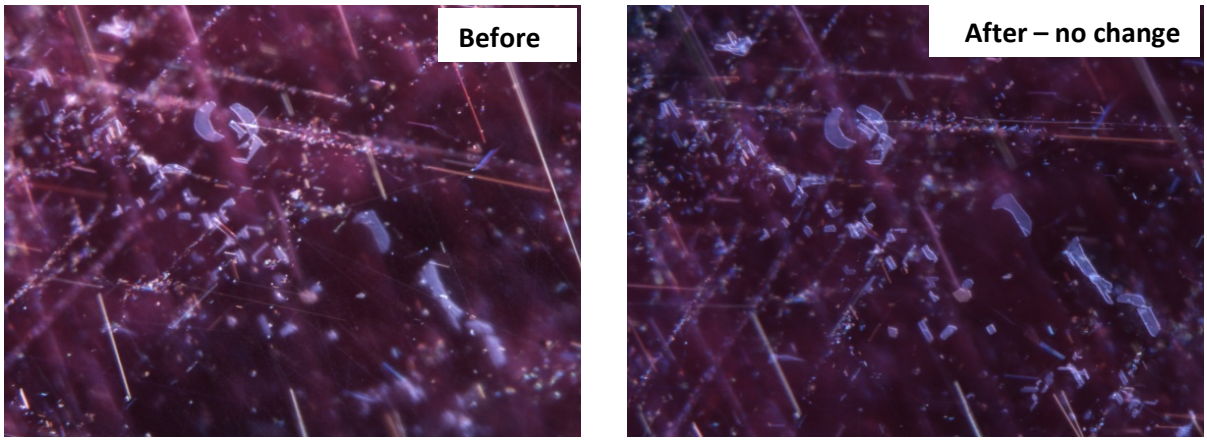

Figure 14: Sample 7054, before (left) and after (right) heat treatment at **800°C for 8 hours.** After heat treatment, there was no sign of alterations in thin films. Fiber-optic illumination. FOV 1.1 mm. Photo: B. Kongsomart © GIA.

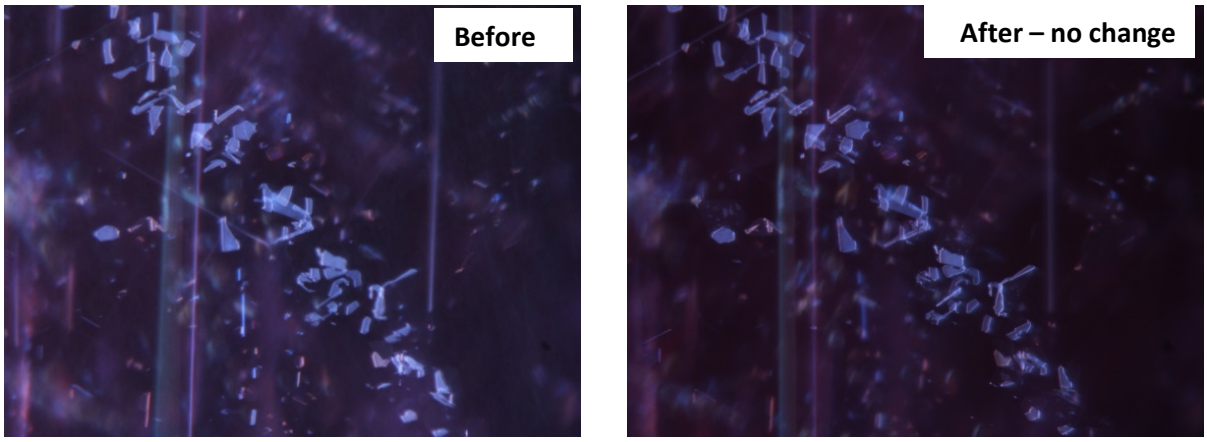

Figure 15: Sample 7054, before (left) and after (right) heat treatment at **800°C for 8 hours.** After heat treatment, there was no change in thin films. Fiber-optic illumination. FOV 0.8 mm. Photo: B. Kongsomart © GIA.

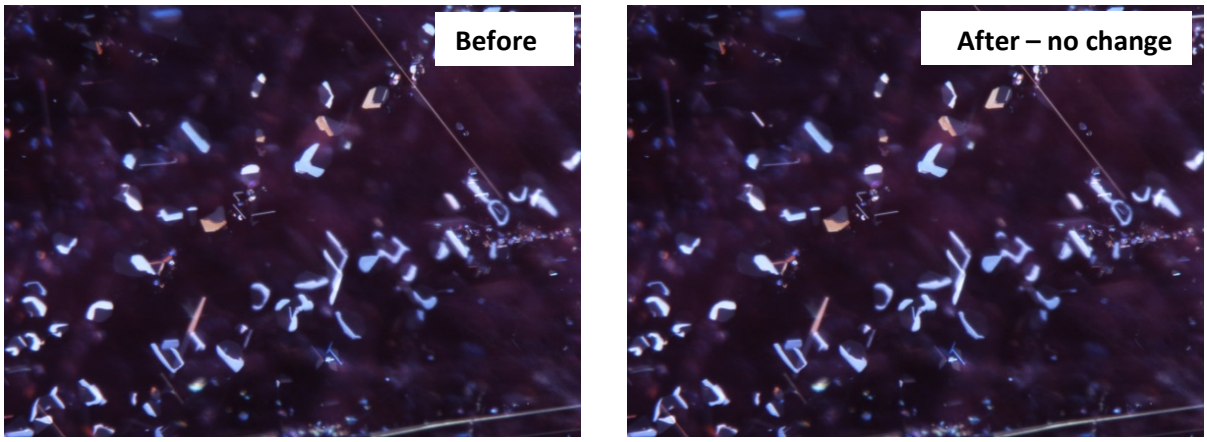

Figure 16: Sample 7100, before (left) and after (right) heat treatment at **800°C for 8 hours**. After heat treatment, there were no changes in the platelets. Fiber-optic illumination. FOV 1.0 mm. Photo: B. Kongsomart © GIA.

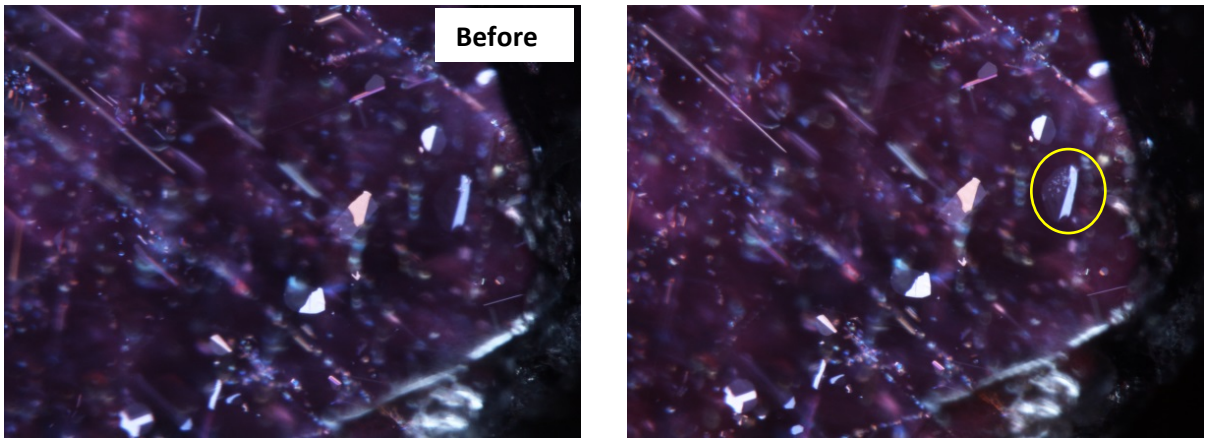

Figure 17: Sample 7100, before (left) and after (right) heat treatment at **800°C for 8 hours**. After heat treatment, some platelets showed a spotty appearance. Fiber-optic illumination. FOV 1.0 mm. Photo: B. Kongsomart © GIA.

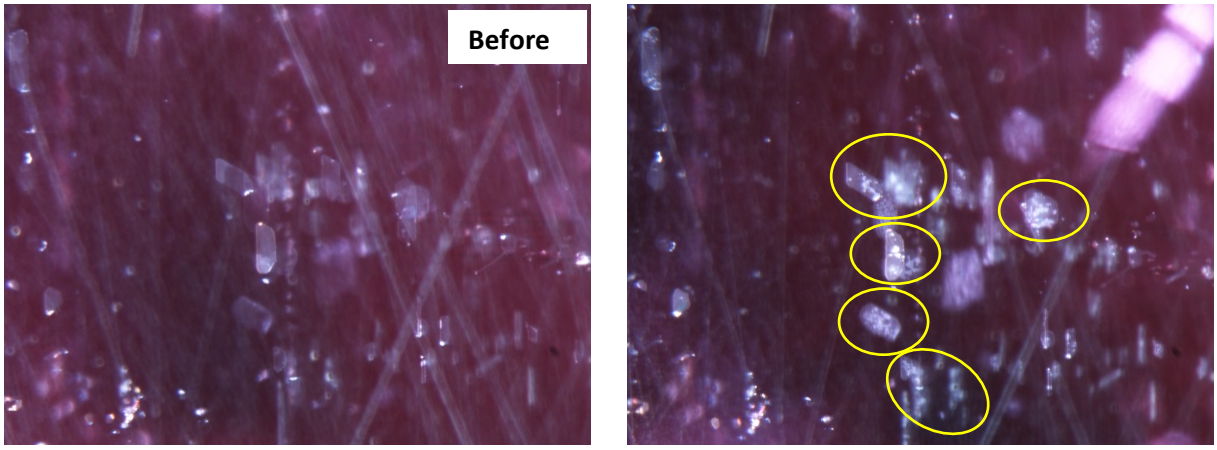

Figure 18: Sample 7097, before (left) and after (right) heat treatment at **800°C for 8 hours**. After heat treatment, the platelets showed bright spots. Fiber-optic illumination. FOV 0.7 mm. Photo: B. Kongsomart © GIA.

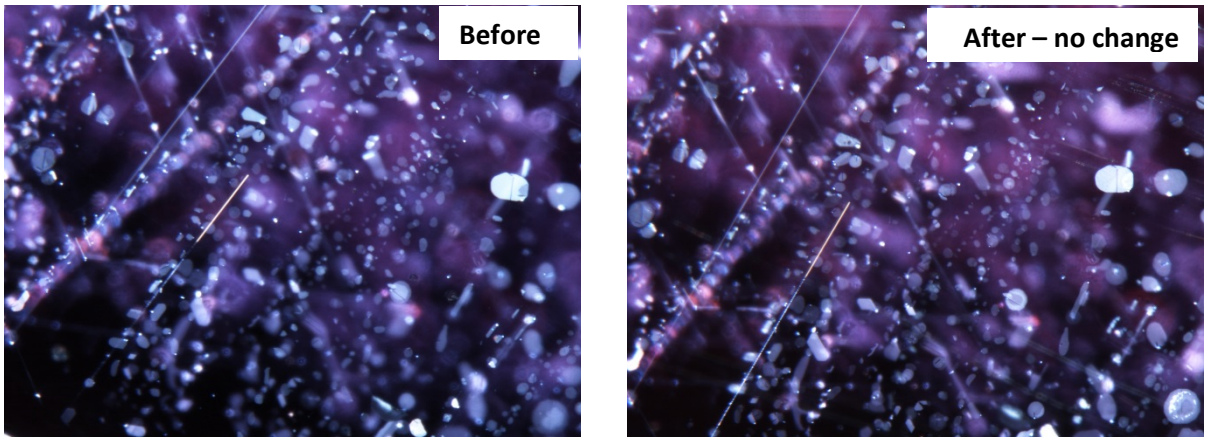

Figure 19: Sample 6569, before (left) and after (right) heat treatment at **800°C for 24 hours**. After heat treatment, none of the platelets changed. Fiber-optic illumination. FOV 1.1 mm. Photo: B. Kongsomart © GIA.

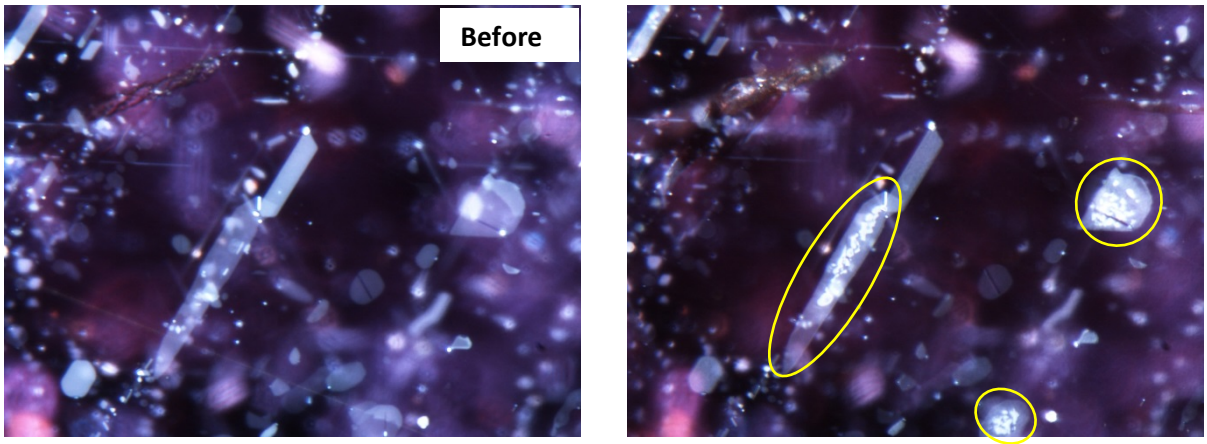

Figure 20: Sample 6569, before (left) and after (right) heat treatment at **800°C for 24 hours**. After heat treatment, many spots appeared on the platelets. Fiber-optic illumination. FOV 0.7 mm. Photo: B. Kongsomart © GIA.

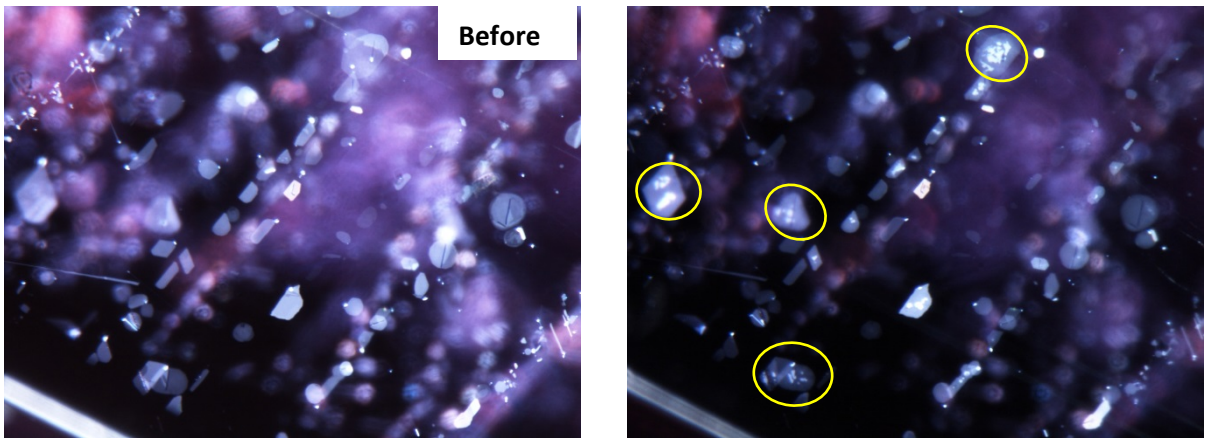

Figure 21: Sample 6569, before (left) and after (right) heat treatment at **800°C for 24 hours**. After heat treatment, the platelets showed bright spots. Fiber-optic illumination. FOV 1.1 mm. Photo: B. Kongsomart © GIA.

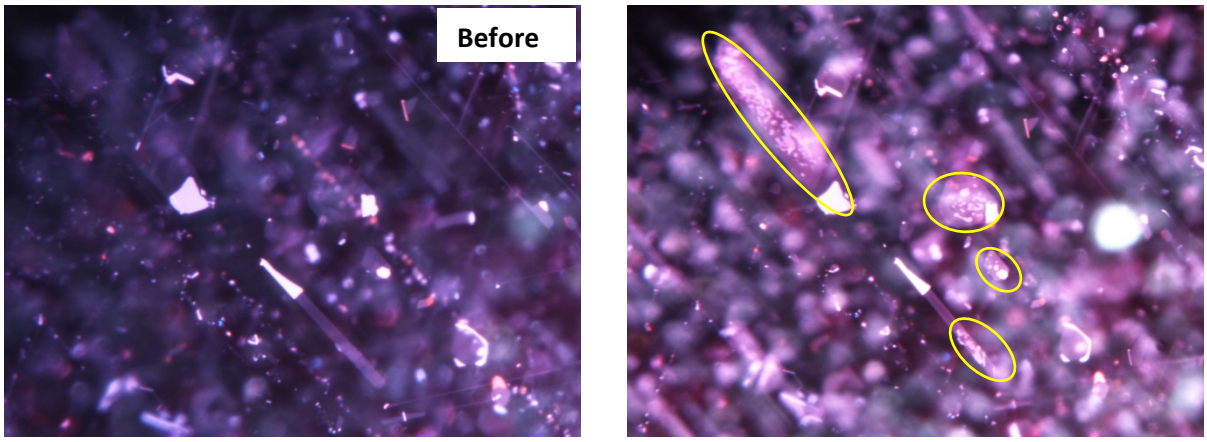

Figure 22: Sample 6569, before (left) and after (right) heat treatment at **800°C for 24 hours.** After heat treatment, the platelets showed many bright spots. Fiber-optic illumination. FOV 1.0 mm. Photo: B. Kongsomart © GIA.

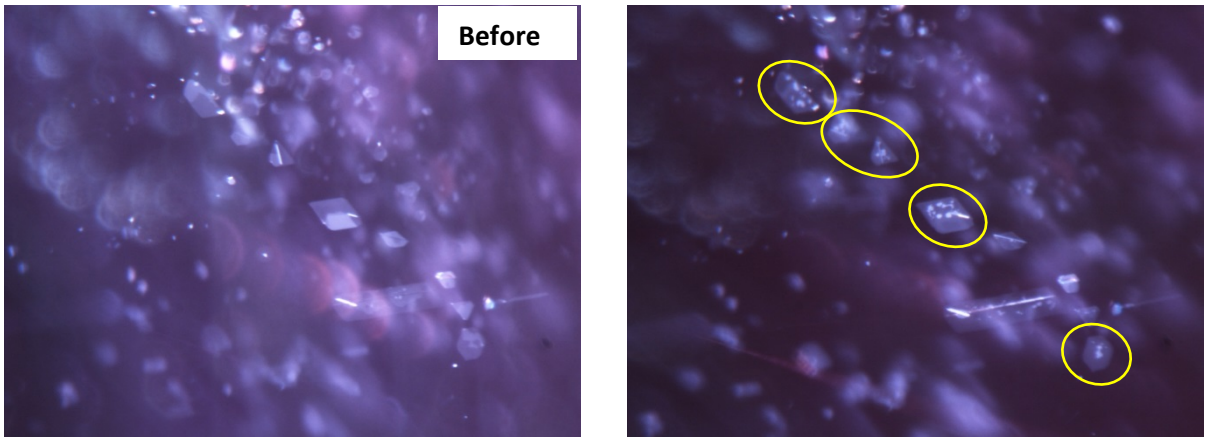

Figure 23: Sample 0911 before (left) and after (right) heat treatment at **800°C for 24 hours**. After heat treatment, the platelets showed a spotty appearance. Fiber-optic illumination. FOV 0.9 mm. Photo: B. Kongsomart © GIA.

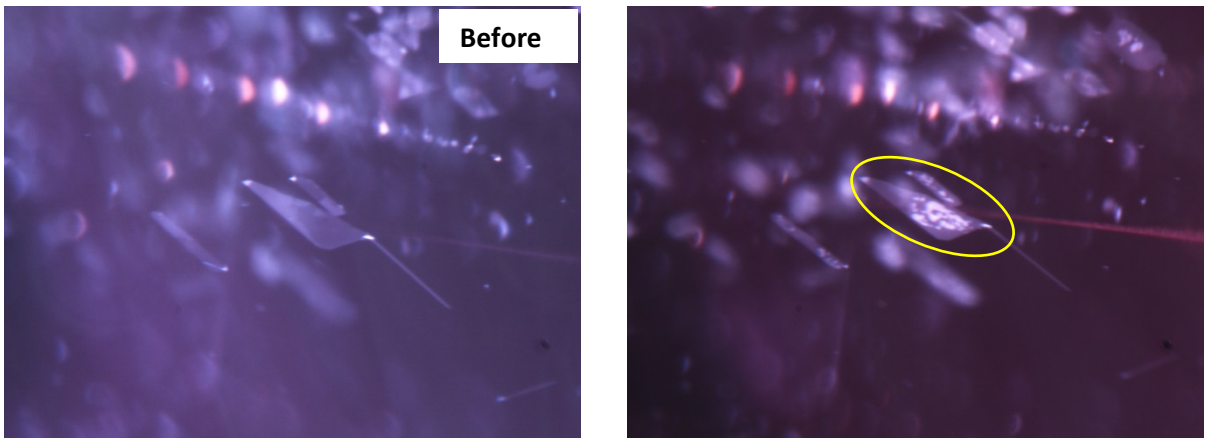

Figure 24: Sample 0911 before (left) and after (right) heat treatment at **800°C for 24 hours.** After heat treatment, the platelets showed a spotty appearance. Fiber-optic illumination. FOV 0.7 mm. Photo: B. Kongsomart © GIA.

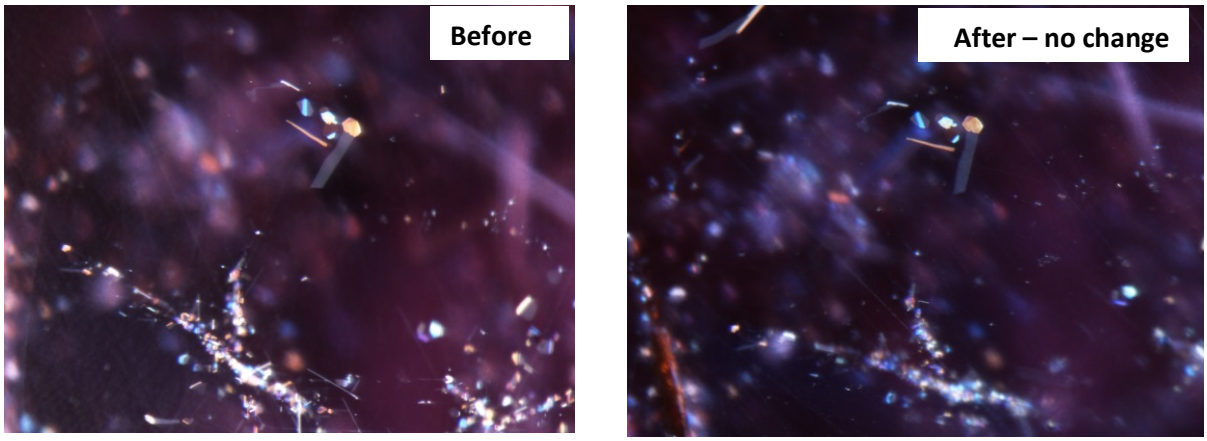

Figure 25: Sample 7026 before (left) and after (right) heat treatment at **900°C for 2 hours and 40 minutes.** After heat treatment, no changes were found in the platelets. Fiber-optic illumination. FOV 0.7 mm. Photo: B. Kongsomart © GIA.

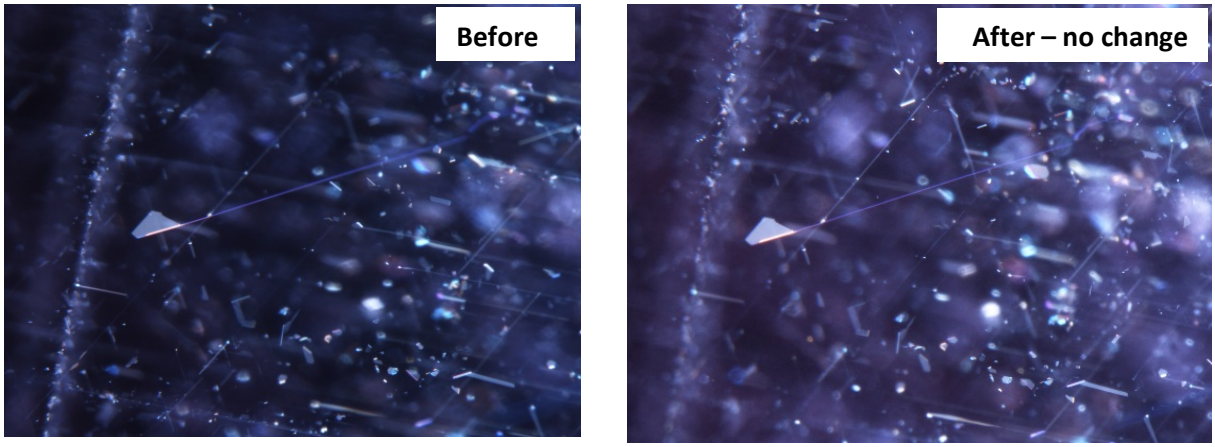

Figure 26: Sample 7074 before (left) and after (right) heat treatment at **900°C, for 2 hours and 40 minutes.** After heat treatment, no changes were found in the platelets. Fiber-optic illumination. FOV 1.3 mm. Photo: B. Kongsomart © GIA.

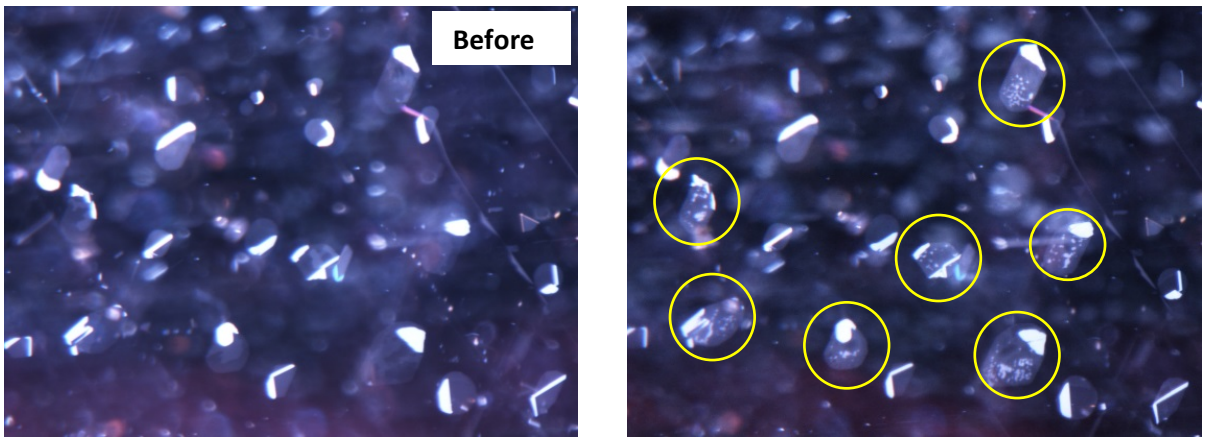

Figure 27: Sample 7074 before (left) and after (right) heat treatment at **900°C for 2 hours and 40 minutes.** After heat treatment, the platelets showed many bright spots. Fiber-optic illumination. FOV 1.0 mm. Photo: B. Kongsomart © GIA.

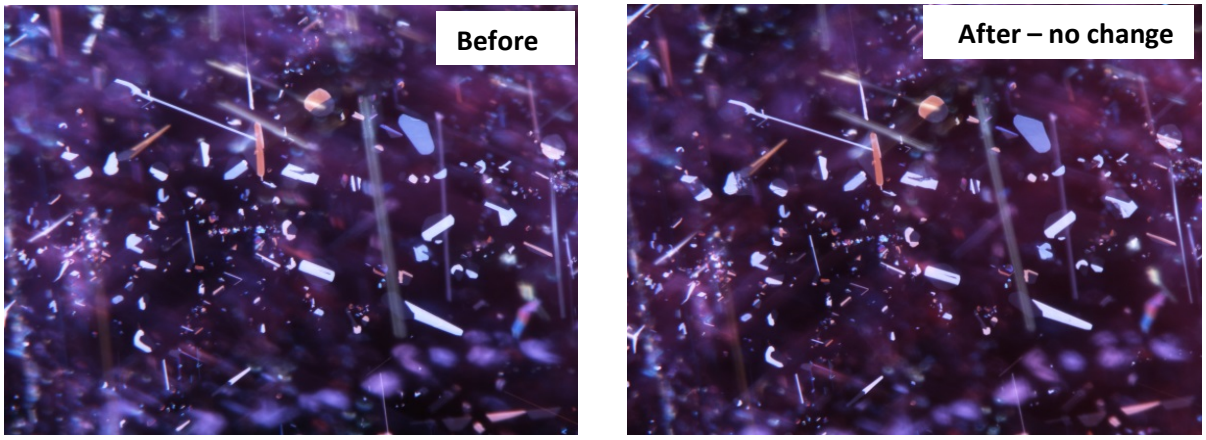

Figure 28: Sample 7005 before (left) and after (right) heat treatment at **900°C for 8 hours.** After heat treatment, no changes were observed. Fiber-optic illumination. FOV 1.3 mm. Photo: B. Kongsomart © GIA.

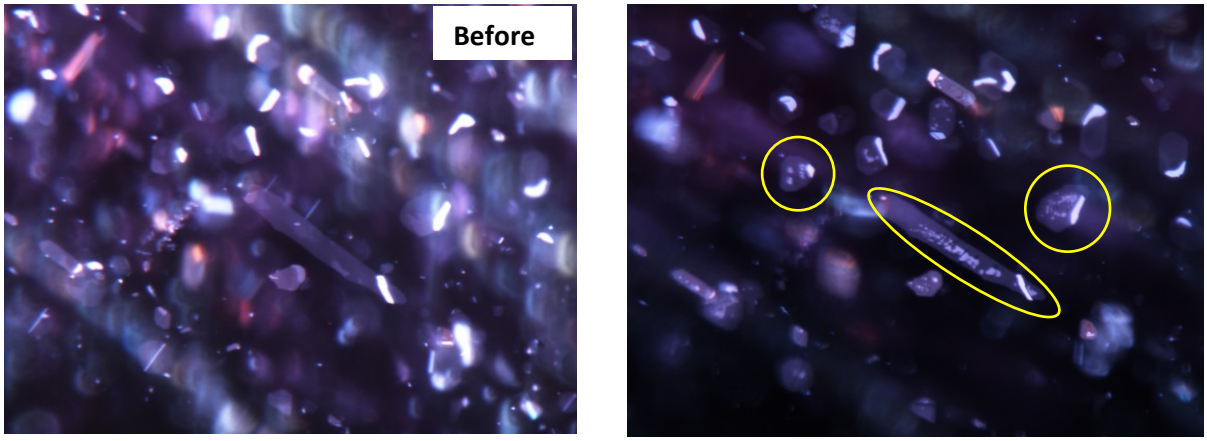

Figure 29: Sample 7040 before (left) and after (right) heat treatment at **900°C for 8 hours.** After heat treatment, many bright spots were created. Fiber-optic illumination. FOV 0.8 mm. Photo: B. Kongsomart © GIA.

EFFECT ON CRYSTALS

Our previous work reported that not all the mineral inclusions seem to be affected in the same manner: Mica, feldspar, and chalcopyrite inclusions appear more likely to be impacted than amphibole or sillimanite inclusions. In this study, only a few samples contained crystal inclusions. We found that amphibole crystals do not show any alteration when heated at 600°C for 24 hours (Figure 30 and Figure 31). However, when samples were heated at 800°C for 24 hours, some (but not all) amphibole crystals developed a discoid fracture around the crystal (Figure 36). Larger crystals seemed to be affected by heat treatment before smaller crystals. Chalcopyrite showed a tension fracture (Figure 35), and mica crystals exhibited discoid fractures after heat treatment (Figure 34 andFigure 37).

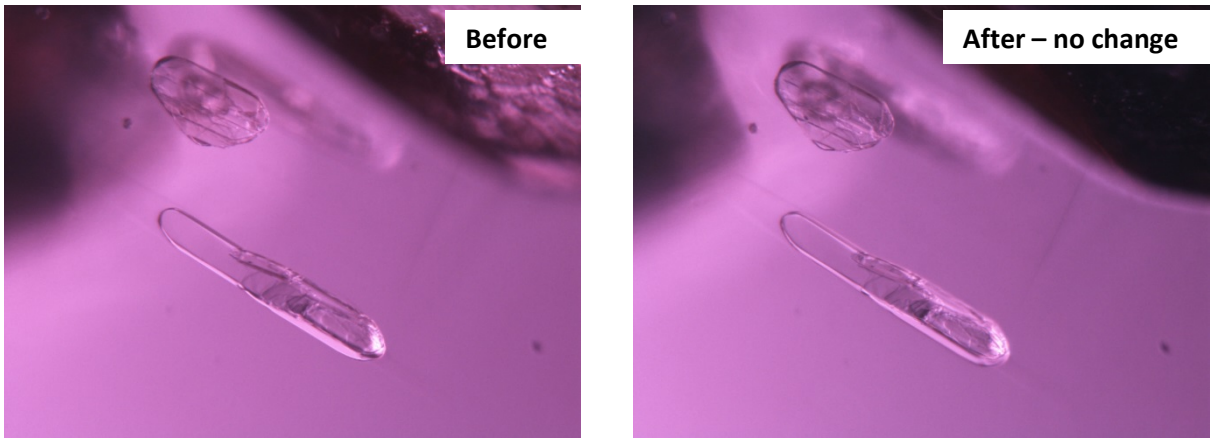

Figure 30: Sample 6599, before (left) and after (right) heat treatment at **600°C for 24 hours**. Amphibole crystals showed no visible changes after heat treatment. Brightfield illumination. FOV 0.9 mm. Photo: B. Kongsomart © GIA.

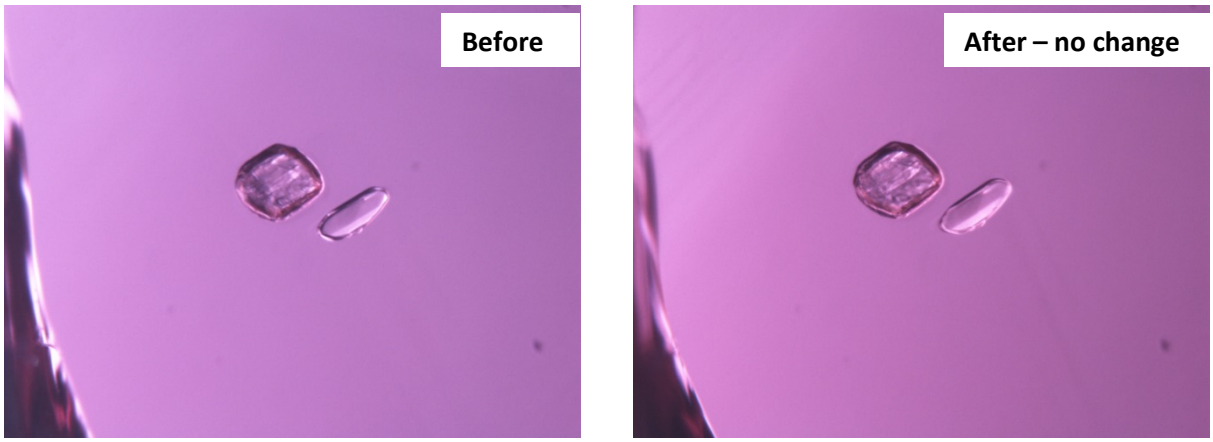

Figure 31: Sample 6599, before (left) and after (right) heat treatment at **600°C for 24 hours**. Amphibole crystals showed no change after heat treatment. Brightfield illumination. FOV 1.0 mm. Photo: B. Kongsomart © GIA.

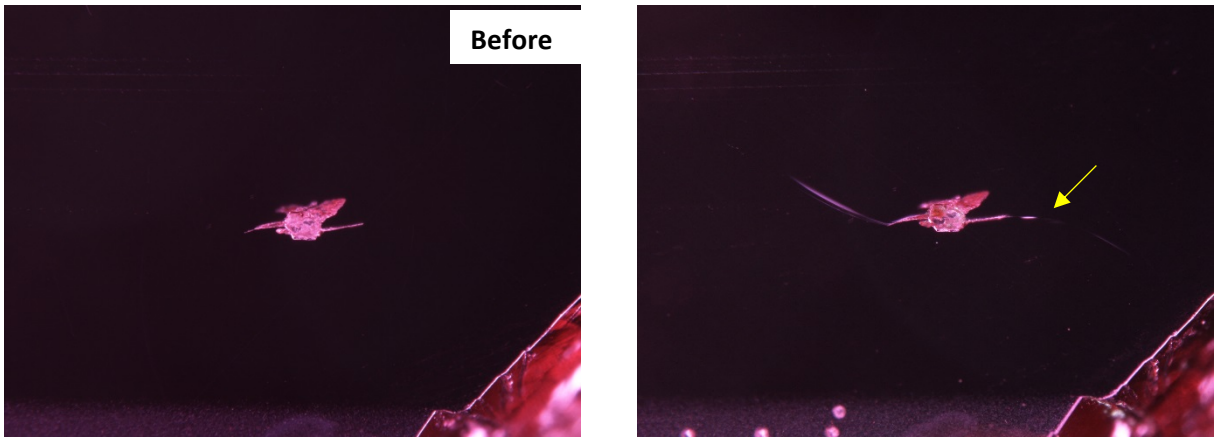

Figure 32: Sample 7076, before (left) and after (right) heat treatment at **700°C for 8 hours**. This crystal (possible mica) showed tension fractures after heat treatment. Darkfield illumination. FOV 2.7 mm. Photo: B. Kongsomart © GIA.

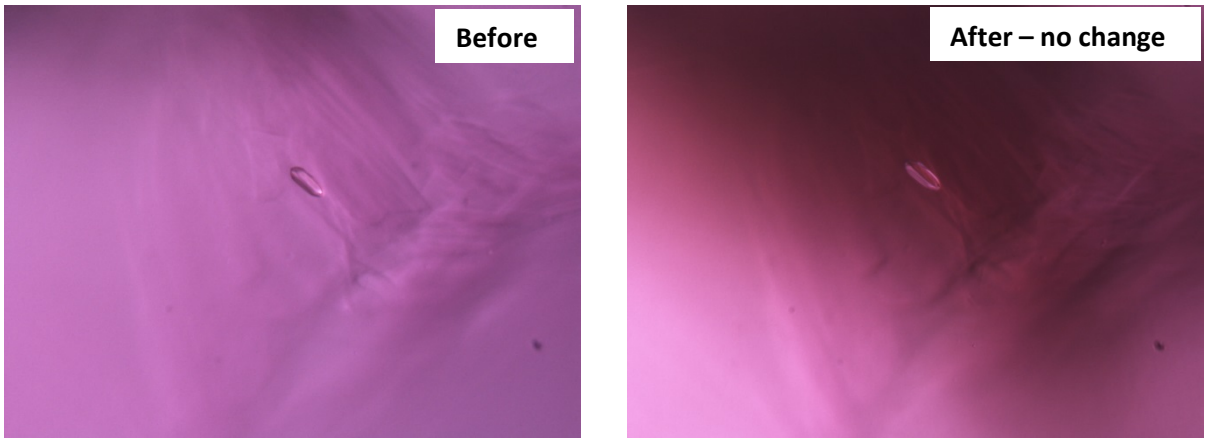

Figure 33: Sample 0911 before (left) and after (right) heat treatment at **800°C for 24 hours**. After heat treatment, there was no change to this unidentified crystal. Fiber-optic illumination. FOV 0.7 mm. Photo: B. Kongsomart © GIA.

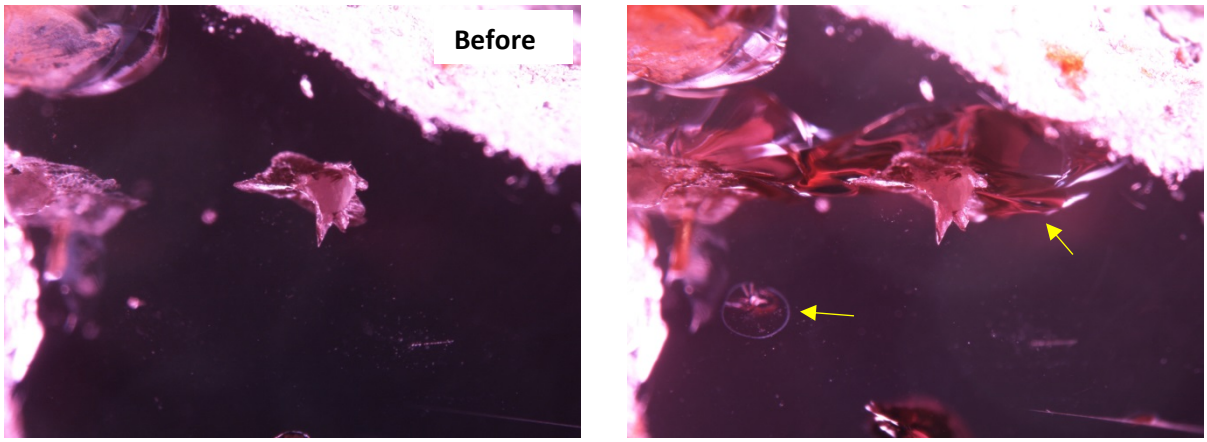

Figure 34: Sample 0911 before (left) and after (right) heat treatment at **800°C for 24 hours**. After heat treatment, this opaque crystal developed fractures that were filled with an opaque substance. Fiber-optic illumination. FOV 4.0 mm. Photo: B. Kongsomart © GIA.

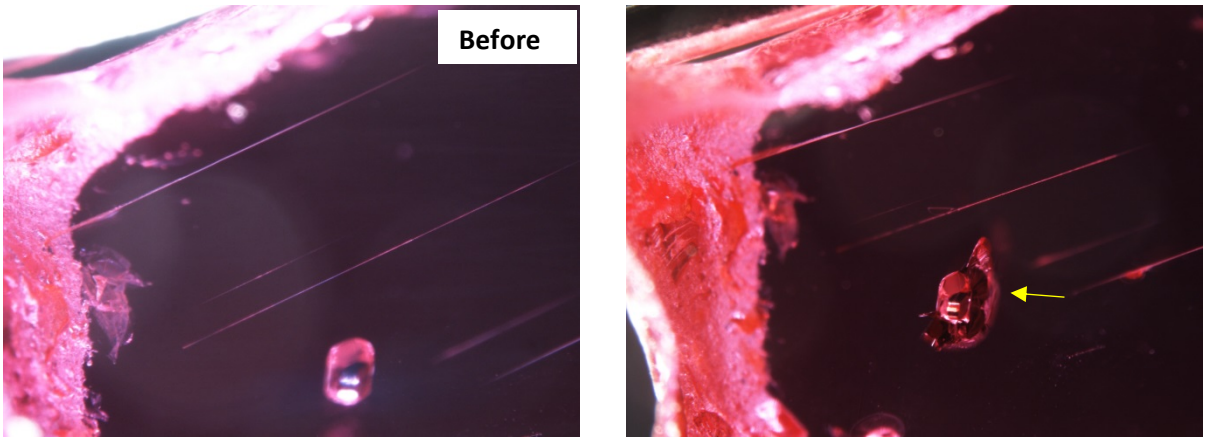

Figure 35: Sample 0911 before (left) and after (right) heat treatment at **800°C for 24 hours**. After heat treatment, this opaque crystal (probably chalcopyrite) developed tension fissures. Fiber-optic illumination. FOV 4.0 mm. Photo: B. Kongsomart © GIA.

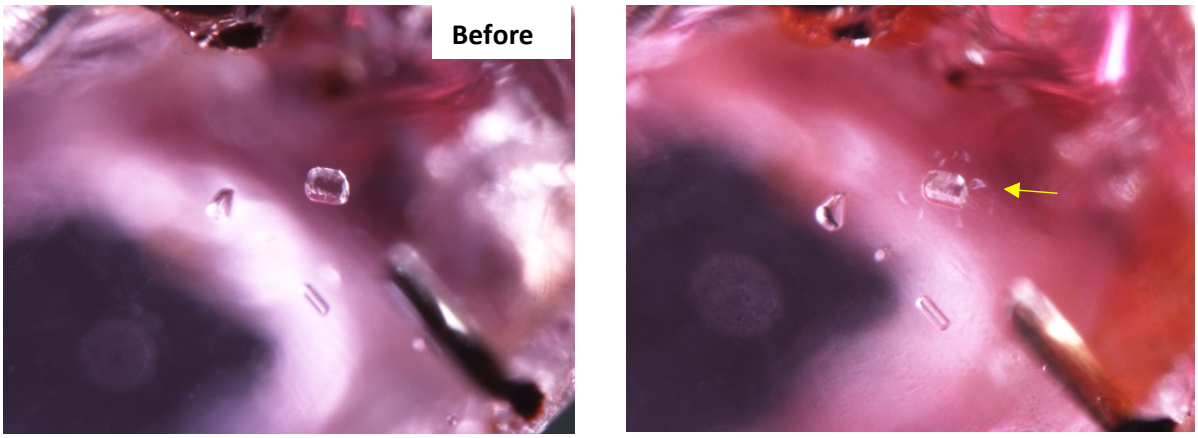

Figure 36: Sample 7074 before (left) and after (right) heat treatment at **900°C for 2 hours and 40 minutes**. After heat treatment, two amphibole crystals did not change whereas a larger amphibole crystal developed discoid fractures (see arrow). Fiber-optic illumination. FOV 1.6 mm. Photo: B. Kongsomart © GIA.

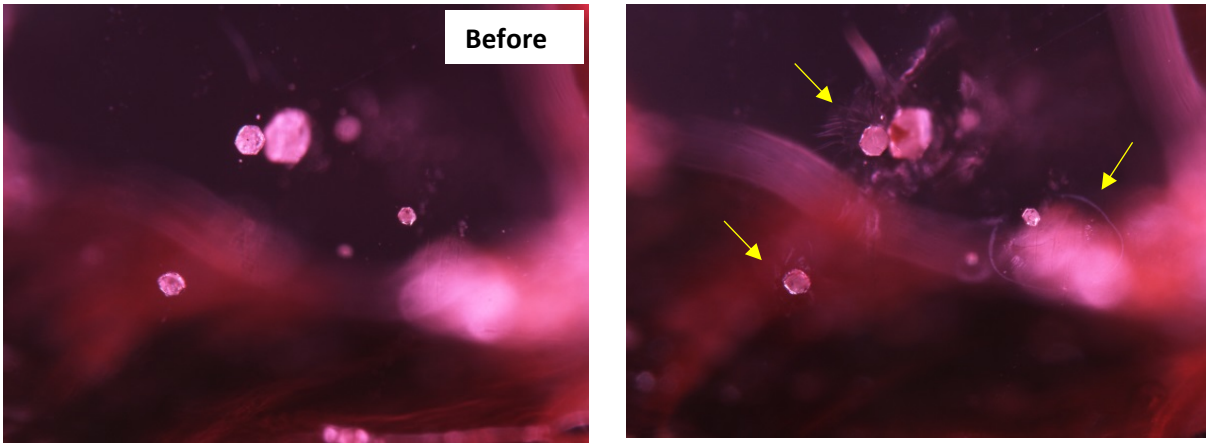

Figure 37: Sample 7040 before (left) and after (right) heat treatment at **900°C for 8 hours**. After heat treatment, these crystals (probably mica) showed discoid fractures. Fiber-optic illumination. FOV 1.6 mm. Photo: B. Kongsomart © GIA.

EFFECT ON NEEDLES

Rutile needles are strongly altered by heat treatment at higher temperature of about 1200–1350°C. In this study, none of the samples showed altered needles or particles, as seen in Figure 38–Figure 42.

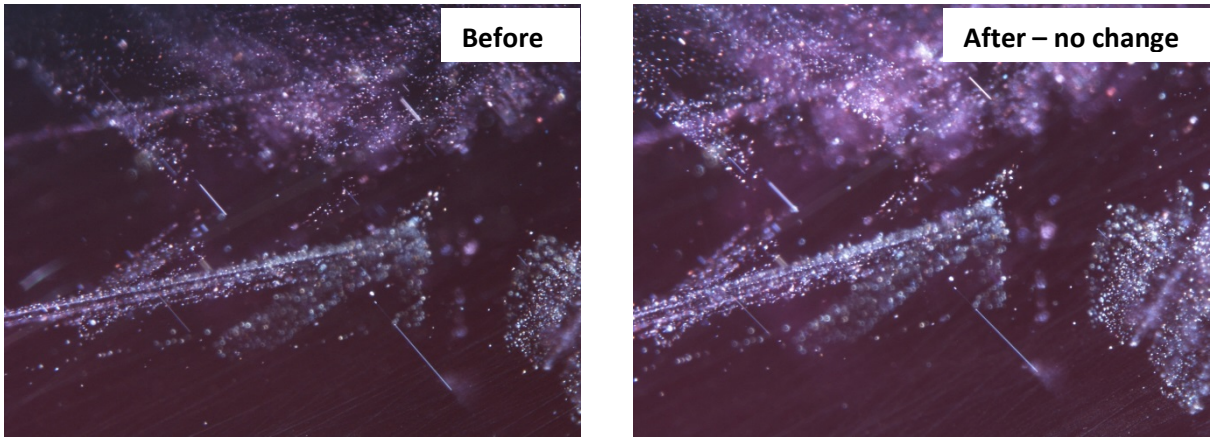

Figure 38: Sample 6599, before (left) and after (right) heat treatment at **600°C for 24 hours**. Clouds of particles and needles showed no difference. Fiber-optic illumination. FOV 1.6 mm. Photo: B. Kongsomart © GIA.

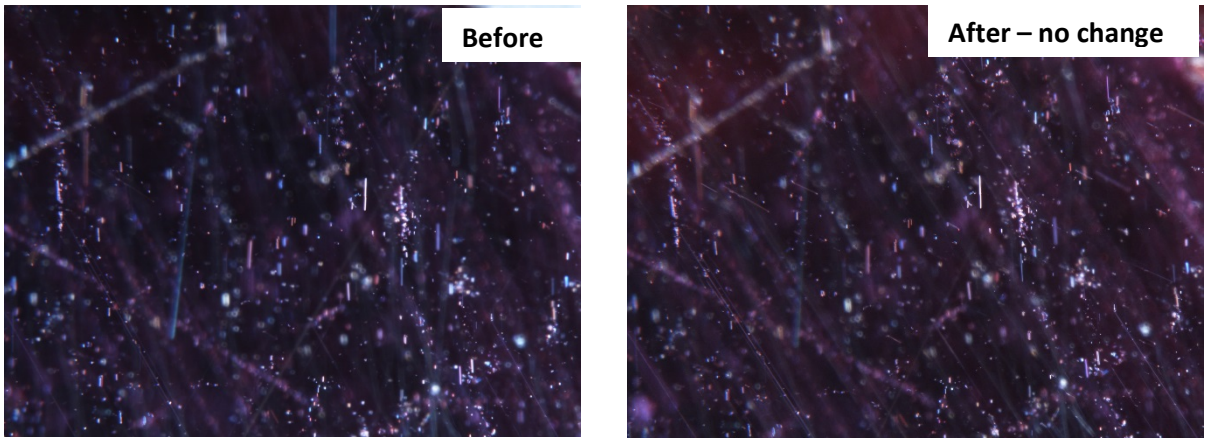

Figure 39: Sample 7008, before (left) and after (right) heat treatment at **700°C for 24 hours**. Short needles showed no changes after heat treatment. Fiber-optic illumination. FOV 1.5 mm. Photo: B. Kongsomart © GIA.

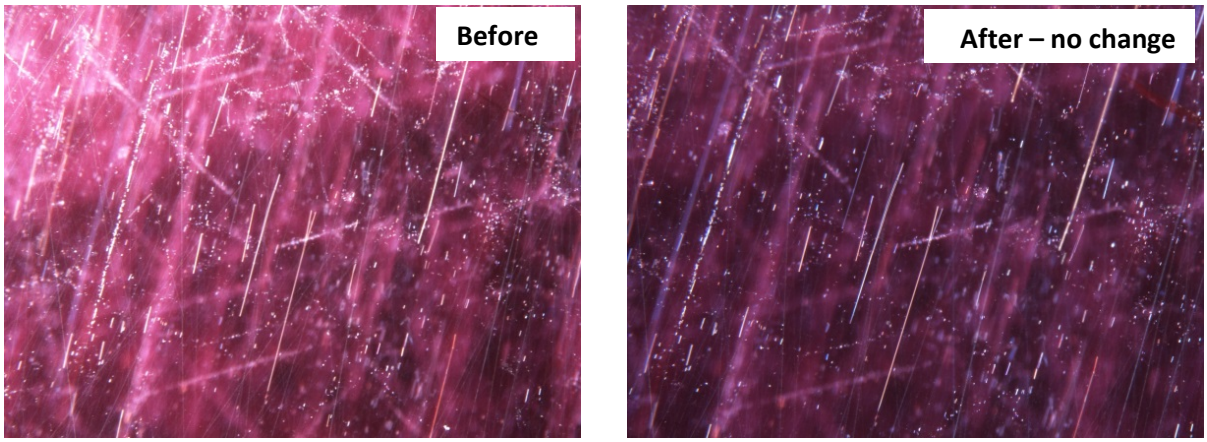

Figure 40: Sample 7054, before (left) and after (right) heat treatment at **800°C for 8 hours**. After heat treatment, needles and particles showed no changes. Fiber-optic illumination. FOV 2.0 mm. Photo: B. Kongsomart © GIA.

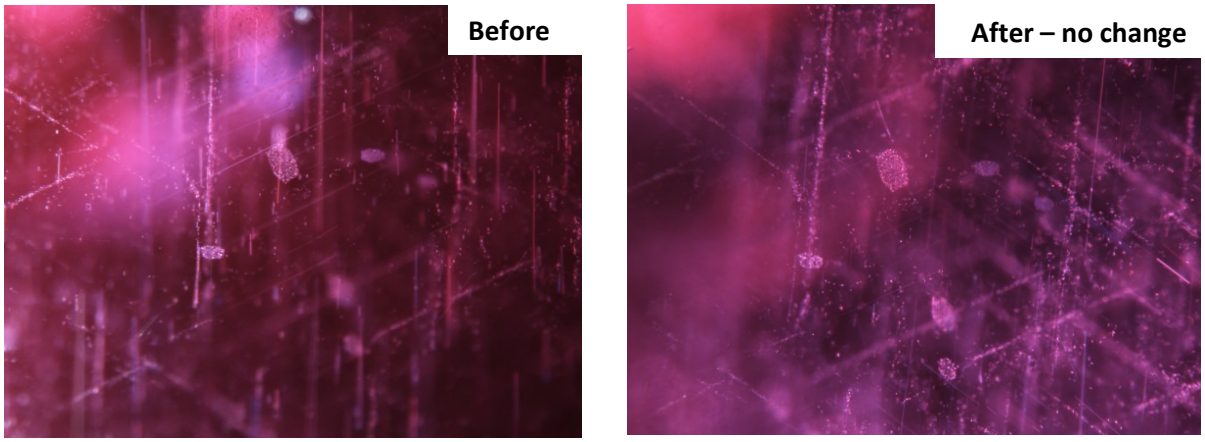

Figure 41: Sample 7054, before (left) and after (right) heat treatment at **800°C for 8 hours**. After heat treatment, needles and groups of particles were not altered. Fiber-optic illumination. FOV 2.0 mm. Photo: B. Kongsomart © GIA.

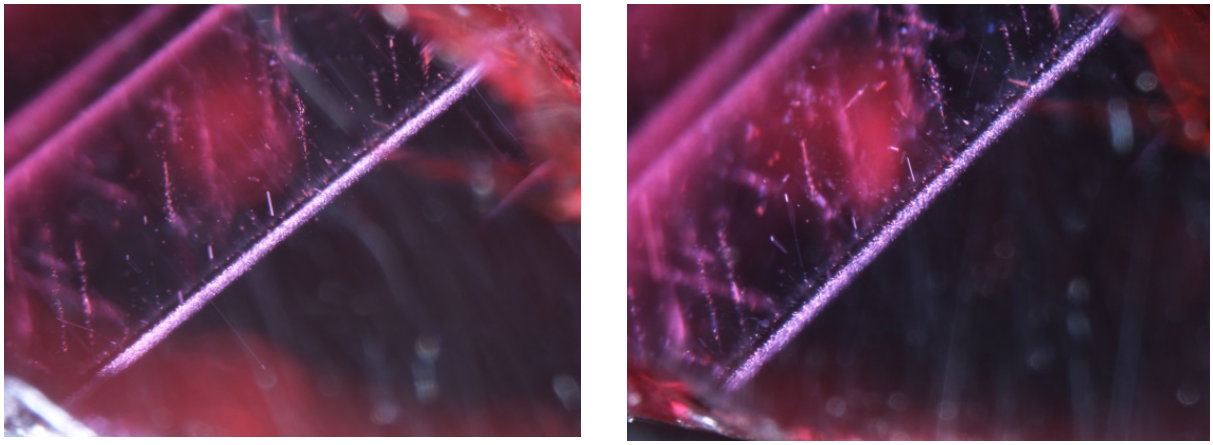

Figure 42: Sample 7026, before (left) and after (right) heat treatment at **900°C, for 2 hours and 40 minutes**. After heat treatment, needles and groups of particles were not altered. Fiber-optic illumination. FOV 2.0 mm. Photo: B. Kongsomart © GIA.

EFFECT ON NATURALLY HEALED FRACTURES OR SURFACE-REACHING FISSURES

We observed that naturally healed fractures are easily affected by heat treatment, often showing expanded tension fractures after treatment (Figure 43). An orange substance in surface-reaching fissures (probably limonite) turned into the darker brownish red hematite after heat treatment (Figure 44Figure 45), which corresponded to previous studies (De Faria and Lopes, 2017; Koivula, 2013; Sripoonjan, 2016).

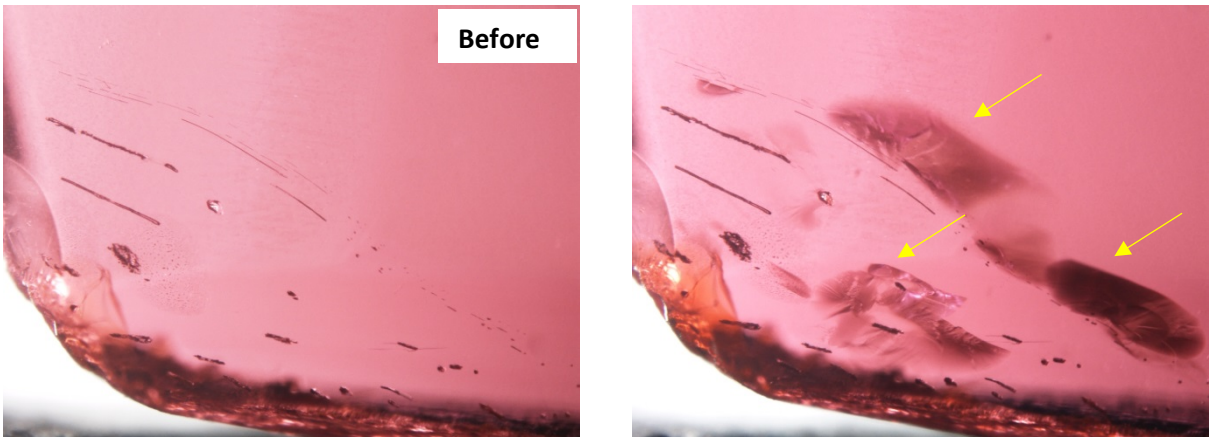

Figure 43: Sample 6579, before (left) and after (right) heat treatment at **600°C for 24 hours**. Fingerprints with tension fractures were found after heat treatment. Brightfield illumination. FOV 2.7 mm. Photo: B. Kongsomart © GIA.

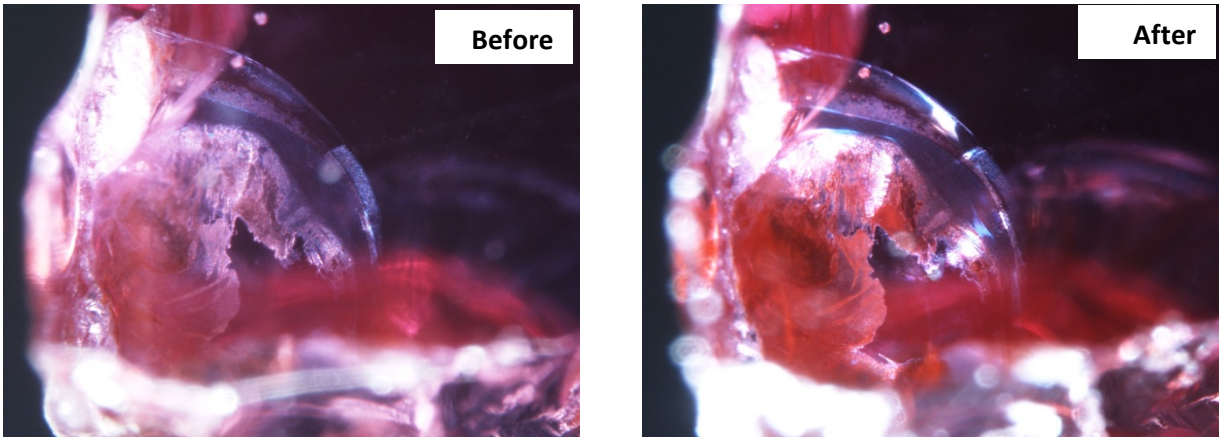

Figure 44: Sample 6599, before (left) and after (right) heat treatment at **600°C for 24 hours**. Fractures filled with an orange foreign substance (reported as limonite) became a darker orangy red (reported as hematite) after heat treatment. Darkfield and fiber-optic illumination. FOV 1.6 mm. Photo: B. Kongsomart © GIA.

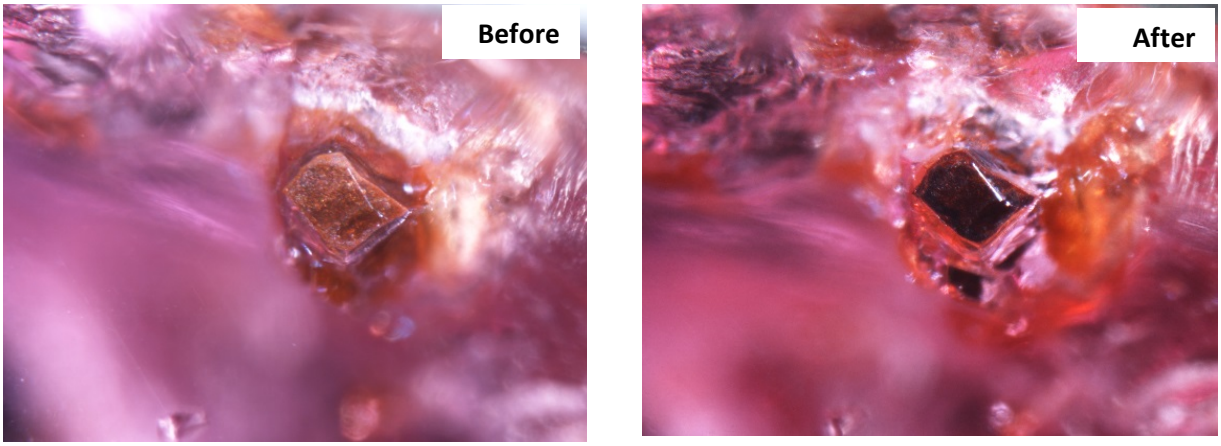

Figure 45: Sample 7074, before (left) and after (right) heat treatment at **900°C for 2 hours and 40 minutes**. Fractures filled with an orange foreign substance (reported as limonite) displayed a darker orangy red (reported as hematite) after heat treatment. Darkfield and fiber-optic illumination. FOV 1.3 mm. Photo: B. Kongsomart © GIA.

During the second experiment, four samples were heated at 800°C for 2 hours and 40 minutes and repeated three consecutive times. All data was collected after heating at each step. We found that only a few platelets changed during this experiment (table 1a), whereas needles or particles were unaffected (table 1b). Crystals developed tension fractures. The results of heating multiple times showed no obvious color or inclusion changes after a second or third heating.

Table 1: Effect of heat treatment on GIA reference sample 7062 after three consecutive heat treatments at 800°C for 2 hours and 40 minutes.

Before Heating	After first heating	After second heating	After third heating
a) platelets – some change			
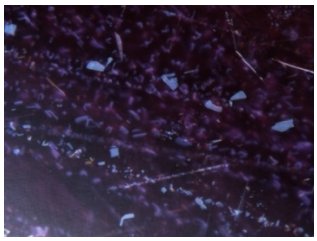	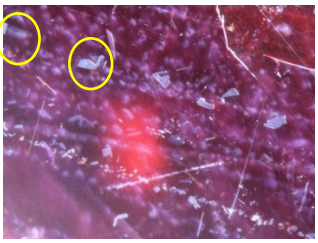	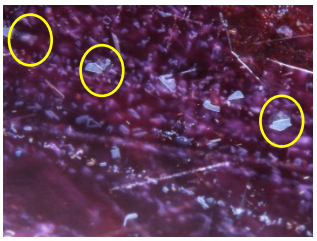	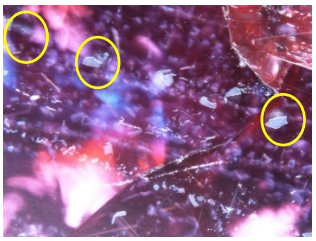
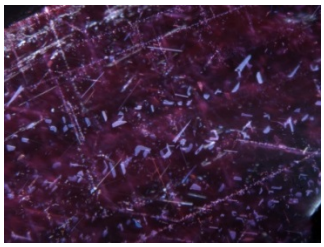		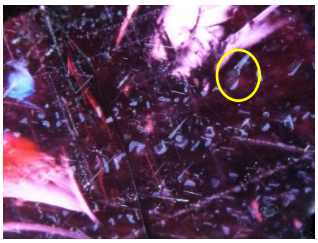	
b) crystals – change			
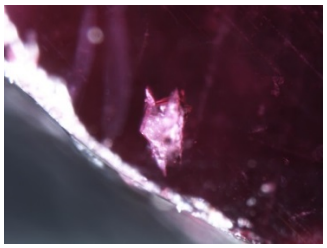	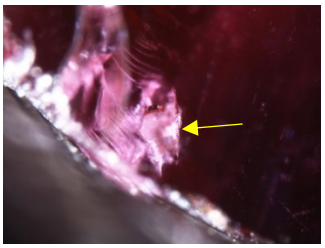	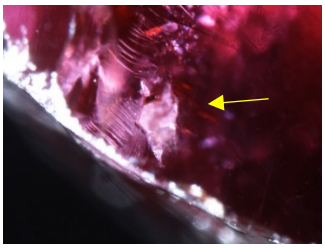	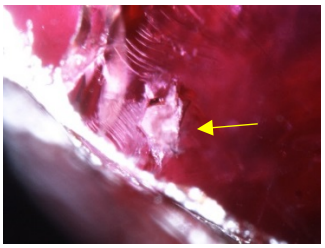
c) needles – no change			
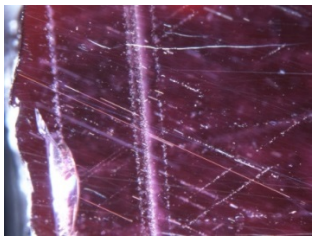	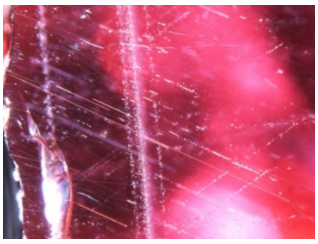	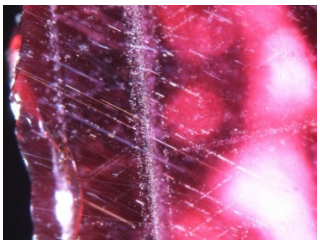	

3.3 Fourier-Transform Infrared (FTIR) Spectroscopy

Infrared spectra were collected in the same area of each sample before and after heat treatment. In our previous report (Pardieu et al., 2015), we observed that a peak at 3309 cm^{-1} decreased in intensity or disappeared, while a peak at 3232 and 3186 cm^{-1} appeared in some samples after heat treatment. A peak at 3161 cm^{-1} was also shown to decrease after heat treatment in samples that showed the peak prior to heat treatment.

Two different experiments were carried out in this study:

1. to observe infrared features at different temperatures and heating durations
2. to confirm the presence of the 3232 cm^{-1} peak after treatment

For the first experiment, samples were heated at 600, 700, 800, and 900°C for 2 hours and 40 minutes, 8, and 24 hours. Results showed that the peak at 3309 cm^{-1} decreased in all samples, while a peak at 3232 cm^{-1} appeared in 11 out of the 24 samples after heat treatment. As Table 2 shows, samples heated at 600°C for 24 hours showed a slightly smaller peak at 3309 cm^{-1} and did not reveal a peak at 3232 cm^{-1}. The peak was only detected when the samples were heated at 700°C or higher temperatures. However, the 3232 cm^{-1} peak only forms when the height of the peak at 3309 cm^{-1} is greater than 0.04 cm^{-1}. For example, heating GIA reference sample 7019 at 800°C for 2 hours and 40 minutes did not produce a 3232 cm^{-1} peak because the height of the 3309 cm^{-1} peak was only about 0.02 cm^{-1} before heat treatment. In contrast, GIA reference sample 7036 presented the 3232 cm^{-1} peak after heating because the peak at 3309 cm^{-1} was about 0.11 cm^{-1} before heat treatment; see Figure 46.

We also collected infrared spectra after the samples were heated at 800°C for 2 hours and 40 minutes and repeated the treatment three times. Results showed no significant differences between the first, second, and third steps of heat treatment (see Table 3).

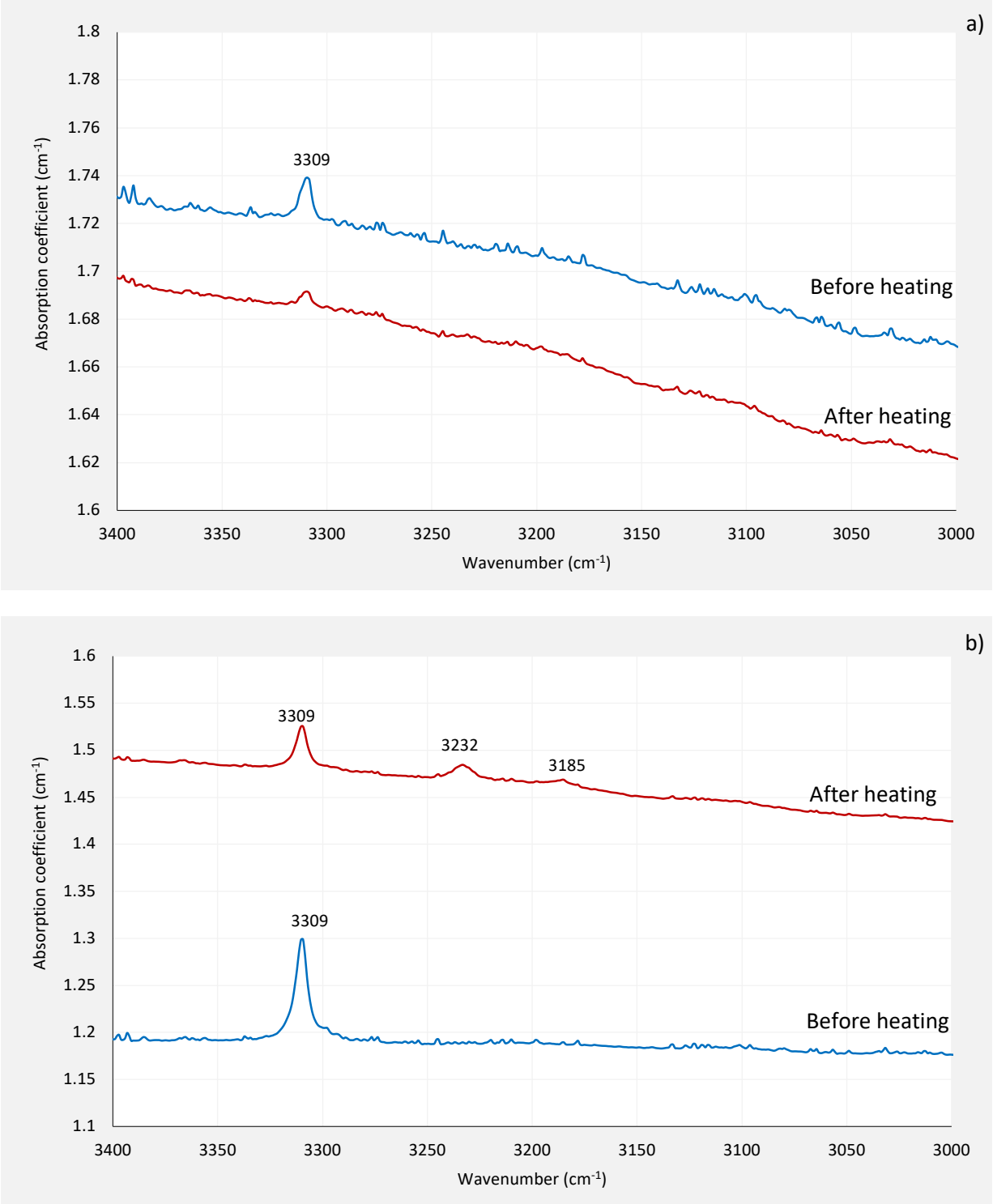

Figure 46: Comparison of FTIR spectra before and after heat treatment at **800°C for 2 hours and 40 minutes** on GIA reference sample 7019 and 7036 in the 3400–3000 cm^{-1} range. Optical path length: 2.608 mm and 3.181 mm, respectively. *Without the polarizer in the FTIR spectrometer, it was not possible to obtain accurate optical FTIR spectra.

Table 2: FTIR peak and platelet comparison of the GIA samples before and after heat treatment.

		GIA ref samples	Peak Height, cm^{-1}				Changes in platelets
			Before heating Peak height in cm^{-1}	After heating Peak height in cm^{-1}			
			3309	3309	3232	3185	
600° C	24 hours	0868	0.0578	0.0544	n/a	n/a	no change
		6566	0.0609	0.0606	n/a	n/a	no change
		6564	0.2055	0.1867	n/a	n/a	no change
		6599	0.0284	0.0280	n/a	n/a	no change
700° C	8 hours	7008	0.0340	0.0275	n/a	n/a	no change
		7094	0.1431	0.1126	0.0076	n/a	no change
	24 hours	6570	0.0363	0.0368	n/a	n/a	change
		6585	0.0252	0.0161	n/a	n/a	change
800° C	2 hours and 40 minutes	7019	0.0183	0.0051	n/a	n/a	slight change
		7036	0.1104	0.0461	0.0147	0.0064	no change
		7062	0.0700	0.0303	0.0099	Present*	slight change
		7077	0.0661	0.0274	0.0099	0.0029	no change
	8 hours	7054	0.1335	0.0522	0.0203	0.0079	no change
		7097	0.0131	0.0057	n/a	n/a	change
		7100	0.0462	0.0188	Present*	n/a	slight change
	24 hours	0911	0.0278	0.0100	0.0036	n/a	change
		6569	0.0357	0.0160	0.0061	n/a	change
900° C	2 hours and 40 minutes	7026	0.0076	n/a	n/a	n/a	no change
		7074	0.0453	0.0129	0.0084	0.0033	change
	8 hours	7005	0.1111	0.0478	0.0298	0.0102	change
		7040	0.0651	0.0149	0.0133	0.0046	change

*"Present" means signal is very close to noise level.
n/a=not detected.

Table 3: FTIR comparison before and after heat treatment with multi-step heating or heat at 800°C for 2 hours and 40 minutes three times.

GIA ref samples (4 samples)	Peak Height (cm^{-1})				Observation
	Before heating	After heating			
	3309	3309	3232	3185	platelets
7019	0.0183	0.0051	n/a	n/a	slight change
7036	0.1104				
After heating; 1st step		0.0461	0.0147	0.0064	no change
2nd step		0.0445	0.0175	0.0061	no change
3rd step		0.0433	0.0185	0.0053	no change
7062	0.0700				
after heating; 1st step		0.0303	0.0099	Present*	slight change
2nd step		0.0283	0.0105	0.0039	Same as 1st step
3rd step		0.0285	0.0115	0.0040	Same as 1st step
7077	0.0661				
after heating; 1st step		0.0274	0.0099	0.0029	no change
2nd step		0.0268	0.0097	0.0034	no change
3rd step		0.0258	0.0111	0.0034	no change

Our second experiment focused on the presence of the 3232 cm^{-1} peak. We noticed that this peak is only present when the intensity of the peak at 3309 cm^{-1} is high. We then selected two groups of samples: (1) 10 samples with small peak height of 3309 cm^{-1} and (2) 10 samples with a large peak of 3309 cm^{-1}. Our results proof that all samples that have a 3309 cm^{-1} peak height higher than about 0.04 cm^{-1} before heat treatment will display the 3232 cm^{-1} peak after treatment. Additionally, we choose three samples with a boehmite and/or kaolinite spectrum (hydrous minerals; Beran et al., 2006) and observed their IR features. Boehmite spectra (3313, 3080, 2110, and 1970 cm^{-1}) completely disappeared (Figure 47a, b) whereas sample 7017 displayed slightly broader peaks (Figure 47c) after heat treatment at 800°C for 2 hours and 40 minutes. Sample 7017 contained many fractures and showed the presence of particles along surface-reaching fractures.

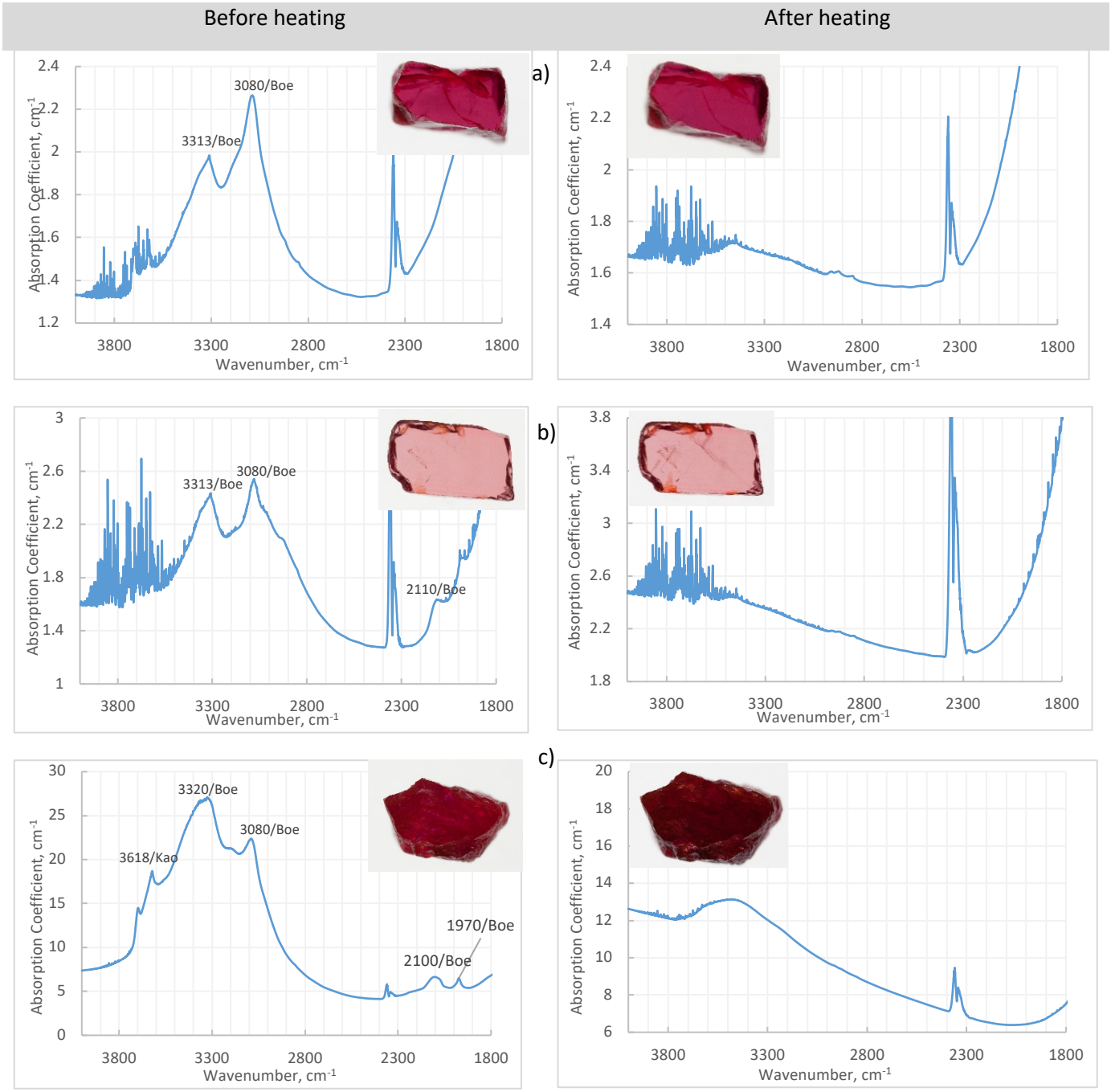

Figure 47: Comparison of FTIR spectra before and after heat treatment at **800°C for 2 hours 40 minutes** on GIA reference samples 7021 (a), 6586 (b), and 7017 (c) in the range between 4000 to 1800 cm^{-1}. Optical path length: 2.595 mm, 2.427 mm, and 0.873 mm, respectively.

It is also interesting to note that FTIR spectroscopy can give different spectra on the same stone and in the same optical direction. For example, GIA reference sample 7057 showed a single 3309 cm^{-1} peak at area A and a smaller peak at 3309 cm^{-1} and the presence of 3161 cm^{-1} on area B (Figure 48a). GIA reference sample #0957 showed the same infrared spectra between two different areas, as shown in Figure 48b.

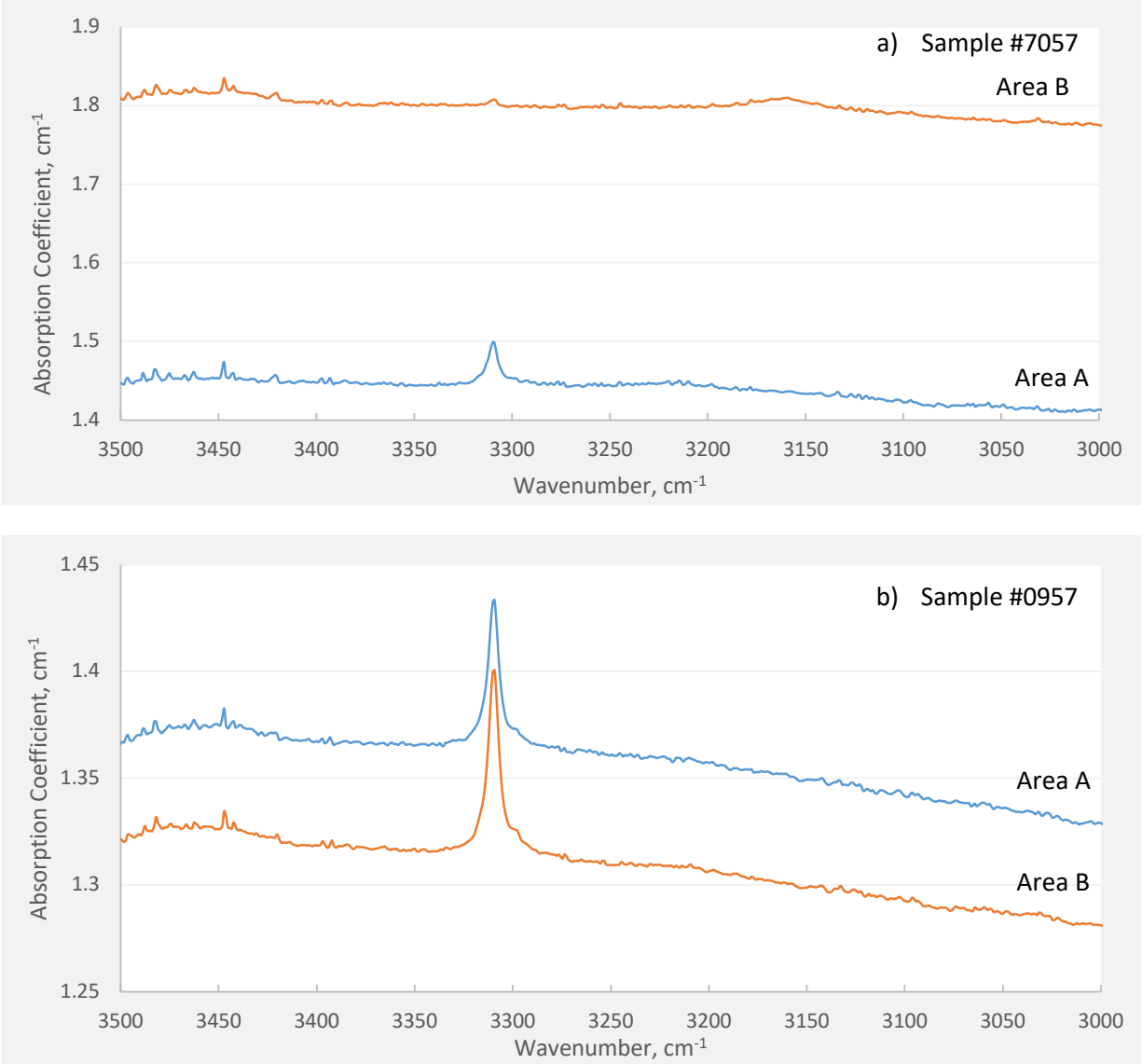

Figure 48: Comparison of FTIR spectra before heat treatment on different areas of GIA reference specimen 7057 and 0957 (each wafer's window was fabricated ⊥ to the c-axis), in the range between 3500 and 3000 cm^{-1}. Optical path length: 1.407 (a) and 1.960 mm (b). *Without the polarizer in the FTIR spectrometer, it was not possible to obtain accurate optical FTIR spectra.

Additionally, we ran infrared spectroscopy on 200 known unheated Mozambique rubies and found no samples presenting a peak at 3232 cm^{-1}. This supports that the 3232 cm^{-1} peak in Mozambican ruby is created by heat treatment.

3.4 UV-Vis-NIR Spectroscopy

GIA reference samples 0957 and 0568 were fabricated with windows parallel or perpendicular to the c-axis. This allowed us to study UV-Vis-NIR spectra at the same area of each sample before and after heat treatment (Emmett et al., 1993).

Sample 0957 exhibited Cr absorption spectra with two broad bands at about 408 and 580 nm and Cr lines at about 475 and 693 nm. Fe absorption spectra peaks at 377, 388, and 450 nm that are related to Fe^{3+} absorption (Ferguson, 1971, 1972) were also recorded.

Before heat treatment, a Cr absorption band at 560 nm was slightly smaller than the Cr absorption band at 410 nm. After heat treatment, the broad band at 560 nm was dramatically reduced. This coincides with a reduction of the broad absorption band at about 580 nm, caused by Fe^{2+}-Ti^{4+} charge transfer, that decreased a blue component. We can simply subtract the spectrum obtained before heat treatment from the spectrum after heat treatment (i.e., spectrum A minus spectrum B) to show the difference between them. The difference spectrum Figure 50) displays a broad absorption band related to Fe^{2+}-Ti^{4+} charge transfer or blue component, as expected. It is noted that an absorption band with a maximum peak at about 880 nm develops after heating (see Figure 49).

Sample 0568 Figure 51) shows very similar results. However, this sample does not show the absorption band at about 880 nm after heat treatment. Sample 0568 contained a lower amount of iron than sample 0957, as shown in

Table 4Table 5. Further study is required to understand the peak absorption band at 880 nm which also found in basalt related blue sapphire.

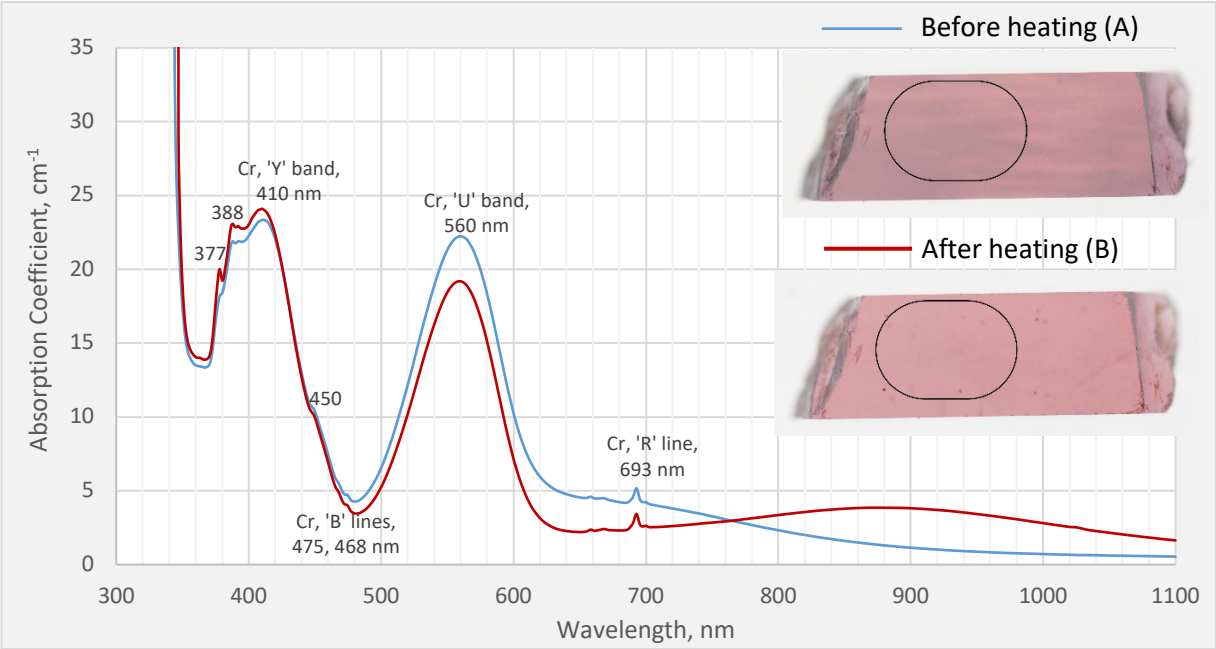

Figure 49: Comparison of ordinary UV-Vis-NIR spectra before and after heat treatment at **800°C for 2 hours 40 minutes** on GIA reference sample 0957. Optical path length: 1.791 mm.

Table 4: LA-ICP-MS results for GIA reference sample 0957 before heat treatment.

GIA reference sample 0957	Concentration (ppma)							
	^{9}Be	^{24}Mg	^{47}Ti	^{51}V	^{53}Cr	^{57}Fe	^{60}Ni	^{69}Ga
sp1	BDL	17	12	4	765	1555	BDL	10
sp2	BDL	16	13	5	808	1643	BDL	11
sp3	BDL	15	27	4	820	1610	BDL	11
sp4	BDL	16	13	5	780	1581	BDL	10
sp5	BDL	17	13	5	812	1603	BDL	10
sp6	BQL	16	12	5	784	1599	BDL	10
sp7	BDL	17	12	5	820	1530	BDL	10
sp8	BDL	16	11	4	769	1566	BDL	10
sp9	BDL	15	11	4	761	1566	BDL	10
sp10	BDL	17	12	4	808	1596	BDL	10
sp11	BDL	17	11	5	753	1523	BDL	10
sp12	BDL	16	11	4	757	1552	BDL	10
Average		**16**	**13**	**4**	**786**	**1577**		**10**
SD		**0.63**	**4.45**	**0.13**	**26**	**35**		**0.39**

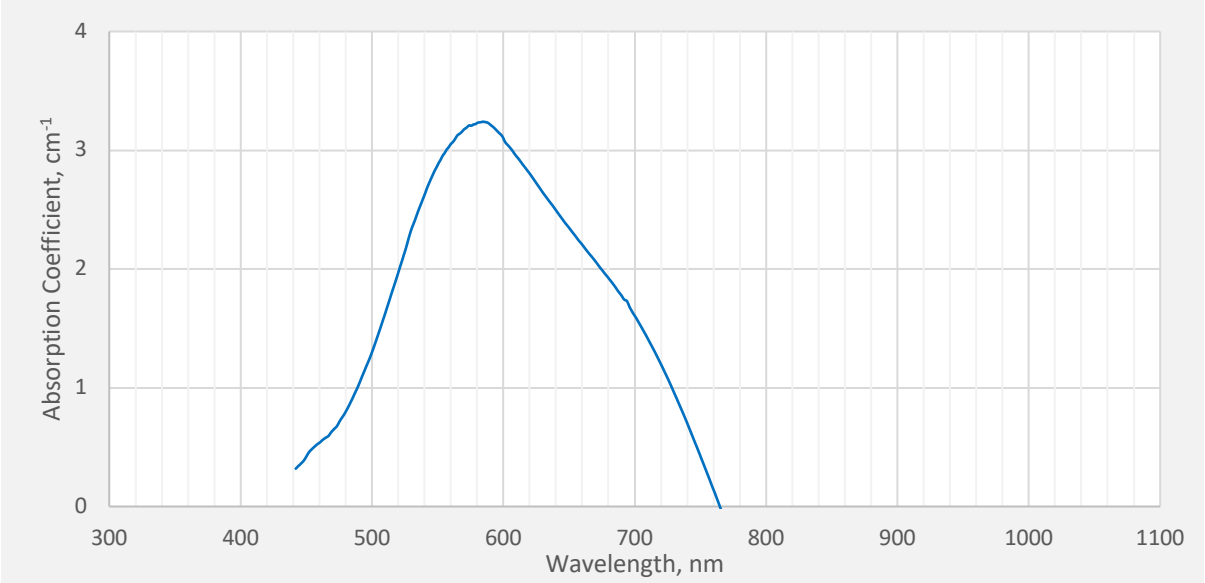

Figure 50: This absorption spectrum is the differential (A minus B) of the two spectra shown in Figure 49. It clearly shows Fe^{2+}-Ti^{4+} absorption.

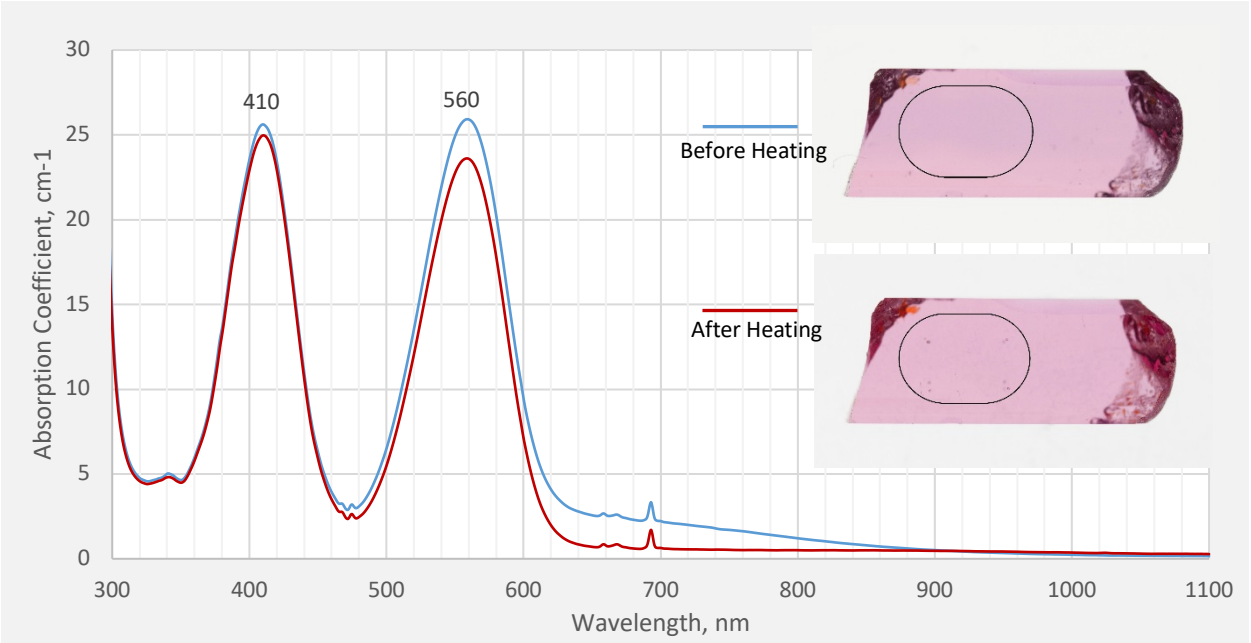

Figure 51: Comparison of ordinary UV-Vis-NIR spectra before and after heat treatment at **800°C for 2 hours 40 minutes** on GIA reference sample 0568. Optical path length: 1.037 mm.

Table 5: LA-ICP-MS results for GIA reference sample 0568 before heat treatment.

GIA reference sample 0568	Concentration in ppma							
	^{9}Be	^{24}Mg	^{47}Ti	^{51}V	^{53}Cr	^{57}Fe	^{60}Ni	^{69}Ga
sp1	BDL	11	14	2	1090	357	BDL	8
sp2	BDL	9	13	2	1176	359	BDL	8
sp3	BDL	10	13	2	1102	369	BDL	8
sp4	BDL	10	12	2	1082	346	BDL	8
sp5	BDL	10	12	2	1051	339	BDL	7
sp6	BDL	9	11	2	1039	338	BDL	7
sp7	BDL	10	12	2	1075	332	BDL	7
sp8	BDL	9	12	2	1039	336	BDL	7
Average		**12**	**15**	**5**	**794**	**1517**		**10**
SD		**0.49**	**1.73**	**0.8**	**17**	**43**		**0.3**

Summary

Mozambique is one of the main producers of ruby at the moment. The Montepuez area produces gems in various sizes and qualities ranging from low-grade commercial to exceptionally high–quality material. Heat treatment is commonly used to improve the quality. It was quickly discovered that Mozambican ruby reacts very well to low-temperature treatment.

During our experiments we could see that blue color zones can be reduced at fairly low temperatures. Detecting this treatment is very challenging because the lower temperatures have less effect on inclusions. Very often, inclusions in Mozambican rubies are limited to needles, platelets, and other fine particles. Sometimes these inclusions are altered very subtly. During treatment, spots can form on these platelets, although this is not always the case. When crystal inclusions are present, it is easier to identify heat treatment because fractures develop around them, especially when the crystals are larger. Some gems contain fractures with iron staining or fingerprints whose appearance can change drastically during treatment.

Since inclusion studies are not conclusive, we must turn to more advanced technology to detect heat treatment. FTIR is the most effective technique for detection. In this study, we concluded that the presence of the 3309, 3232, and/or 3185 cm^{-1} is related to heat treatment. However, the absence of these peaks in the FTIR spectrum does not prove that the stone is not heat treated, since some of the heated stones did not show these peaks. But these peaks are only found in heated stones.

Detection of heat treatment in Mozambican rubies is still very challenging, although new studies and recent developments have led to significant advances. A combination of inclusion study and FTIR spectroscopy can give consistent and accurate results in identifying Mozambican rubies.

ACKNOWLEDGMENTS: The authors thank Dr. John Emmett, Dr. Aaron Palke, Shane McClure, Nicholas Sturman and Duncan Pay, Stuart Overlin, Dr. Tao Z. Hsu for their useful advice and support. We also thank Vincent Pardieu and the field gemology department for sample collection; Sasithorn Engniwat for photo calibration and Charuwan Khowpong and Suwasan Wongchacree for sample fabrication.

ABOUT THE AUTHORS: Sudarat Saeseaw (ssaeseaw@gia.edu) is senior manager of colored stone identification, Boodsakorn Kongsomart is a former research scientist, Ungkhana Atikarnsakul and Charuwan Khowpong are analyst technicians, Wim Vertriest (wvertrie@gia.edu) is a supervisor of field gemology, and Wasura Soonthorntantikul is a research scientist, all at GIA's Bangkok laboratory.

Bibliography

Beran A., Rossman G.R. (2006) OH in naturally occurring corundum. *European Journal of Mineralogy*, Vol. 18, No. 4, pp. 441–447.

De Faria D.L.A., Lopes F.N. (2007) Heated goethite and natural hematite: Can Raman spectroscopy be used to differentiate them? *Vibrational Spectroscopy*, Vol. 45, No. 2, pp. 117–121.

Emmett J.L., Scarratt K., McClure S.F., Moses T., Douthit T.R., Hughes R., Novak S., Shigley J.E., Wang W., Bordelon O., Kane R.E. (2003) Beryllium diffusion of ruby and sapphire. *Gems & Gemology,* Vol. 39, No. 2, pp. 84–135.

Emmett J.L., Douthit T.R. (1993) Heat treating the sapphires of Rock Creek, Montana. *Gems & Gemology*, Vol. 31, No. 2, pp. 250–272.

Ferguson J., Fielding P.E. (1971) The origins of the colours of yellow, green and blue sapphires*. Chemical Physics Letters,* Vol. 10, No. 3, pp. 262–265.

Ferguson J., Fielding P.E. (1972) The origins of the colours of natural yellow, blue, and green sapphires. *Australian Journal of Chemistry*, Vol. 25, pp. 1371–1385.

Hughes R.W., Manorotkul W., Hughes E.B. (2017) *Ruby and Sapphire: A Gemologist's Guide*, 1st edition, RWH Publishing/Lotus Publishing, Thailand.

Koivula J.I. (2013) Useful visual clue indicating corundum heat treatment. *Gems & Gemology*, Vol. 49, No. 3, pp. 160–161.

Nassau K. (1981) Heat treating ruby and sapphire: Technical aspects. *Gems & Gemology*, Vol. 17, No. 3, pp. 121–131.

Pardieu V., Saeseaw S., Detroyat S., Raynaud V., Sangsawong S., Bhusrisom T., Engniwat S., Muyal J. (2015) GIA Lab reports on low-temperature heat treatment of Mozambique ruby. https://www.gia.edu/gia-news-research-low-temperature-heat-treatment-mozambique-ruby.

Pardieu V., Sturman N., Saeseaw S., Du Toit G., Thirangoon K. (2010) FAPFH/GFF treated ruby from Mozambique - A preliminary report. http://www.giathai.net/pdf/Flux_heated_and_glass_filled_rubies_from_Mozambique.pdf.

Pardieu V., Rakotosaona N. (2012) Ruby and sapphire rush near Didy, Madagascar (April - June 2012). http://www.giathai.net/pdf/Didy_Madagascar_TH.pdf.

Pardieu V., Sangsawong S., Muyal J., Chauviré B., Massi L., Sturman N. (2012) Ruby from the Montepuez area (Mozambique) (October 2013). http://www.giathai.net/pdf/GIA_Ruby_Montepuez_Mozambique.pdf.

Sripoonjan T., Wanthanachaisaeng B., Leelawatanasuk T. (2016) Phase transformation of epigenetic iron staining: indication of low-temperature heat treatment in Mozambique ruby. *Journal of Gemmology*, Vol. 35, No. 2, pp. 156–161.

Thomas T. (2009) Corundum c-axis device for sample preparation. http://www.gia.edu/gia-news-research-nr6809

APPENDIX A: Color changes induced in samples after heat treatment

Table A-1: Color-calibrated photo after heat treatment at **600°C for 24 hours in air.**

No.	Before treatment	After treatment	
0868			**No obvious** change to the blue color component Thickness 1.813 mm
6566			**No obvious** change to the blue c color component Thickness 2.104 mm
6568	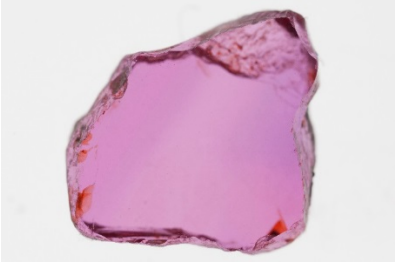	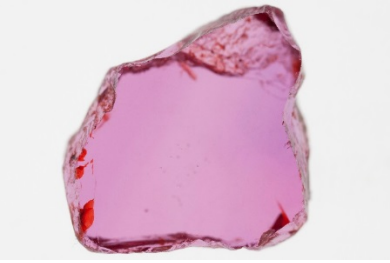	**No obvious** change to the blue color component Thickness 1.722 mm
6579			**No obvious** change to the color Thickness 1.828 mm
6599			**No obvious** change to the blue color component Thickness 1.360 mm

Table A-2: Color-calibrated photo after heat treatment at **700°C for 8 hours in air.**

No.	Before	After	
7008			**No obvious** change to the blue color component Thickness 3.13 mm
7076		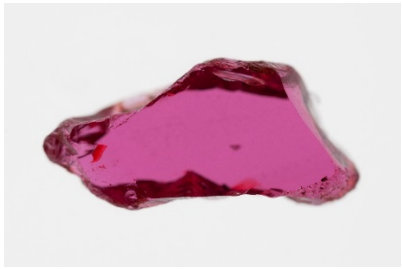	**No obvious** change to the blue color component Thickness 2.04 mm
7094			**No obvious** change to the blue color component Thickness 1.97 mm

Table A-3: Color-calibrated photo after heat treatment at **700°C for 24 hours in air.**

No.	Before	After	
6570			**No obvious** change to the blue color component Thickness 1.99 mm

No.	Before	After	
6585			Blue color **slightly decreased** after heating Thickness 1.33 mm

Table A-4: Color-calibrated photo after heat treatment at **800°C for 8 hours in air.**

No.	Before	After	
7054	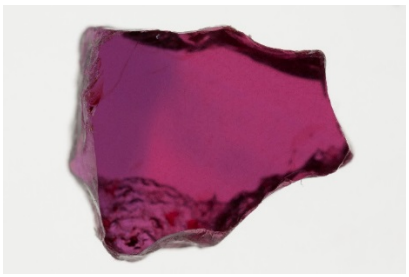	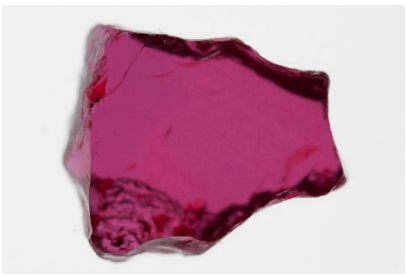	Blue color **decreased** after heating Thickness 2.19 mm
7097			**No obvious** change to the color Thickness 2.13 mm
7100			**No obvious** change to the blue color Thickness 1.65 mm

Table A-5: Color-calibrated photo after heat treatment at **800°C for 24 hours in air.**

No.	Before	After	
0911	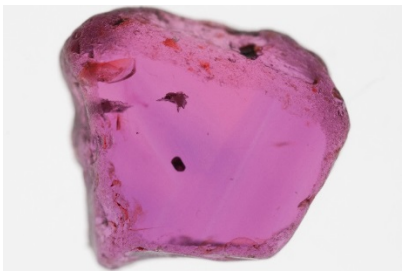		Blue color **decreased** after heating Thickness 2.54 mm
6569 (⊥ c-axis)			Blue color **decreased** after heating Thickness 3.21 mm
6569 (// c-axis)		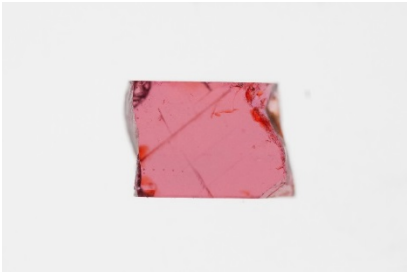	Blue color **decreased** after heating Thickness 1.66 mm

Table A-6: Color-calibrated photo after heat treatment at **900°C for 2 hours and 40 minutes in air.**

No.	Before	After	
7026	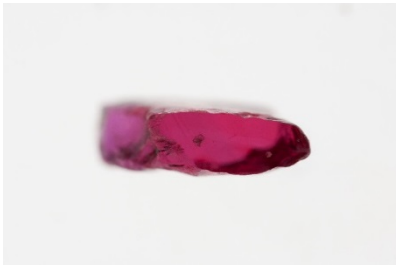	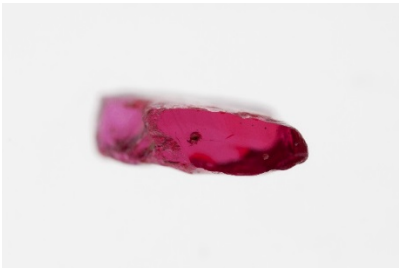	**No obvious** change to the blue color Thickness 3.31mm
7074	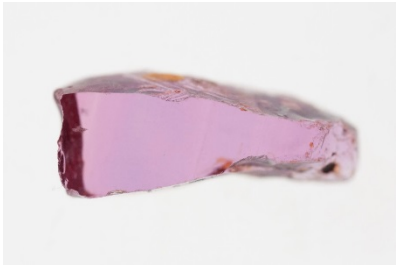	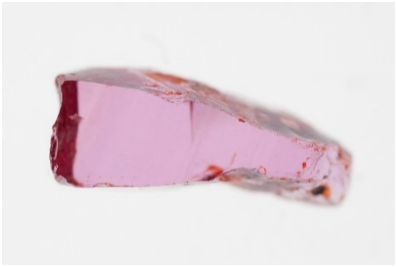	Blue color **decreased** after heating Thickness 3.31mm

Table A-7: Color-calibrated photo after heat treatment at **900°C for 8 hours in air.**

No.	Before	After	
7005			Blue color **decreased** after heating Thickness 3.40 mm
7040			Blue color **decreased** after heating Thickness 1.95 mm

Table A-8: Color-calibrated photo after heat treatment on GIA reference sample #7036 after heating at **800°C for 2 hours and 40 minutes** in air for three consecutive times (thickness 3.181 mm).

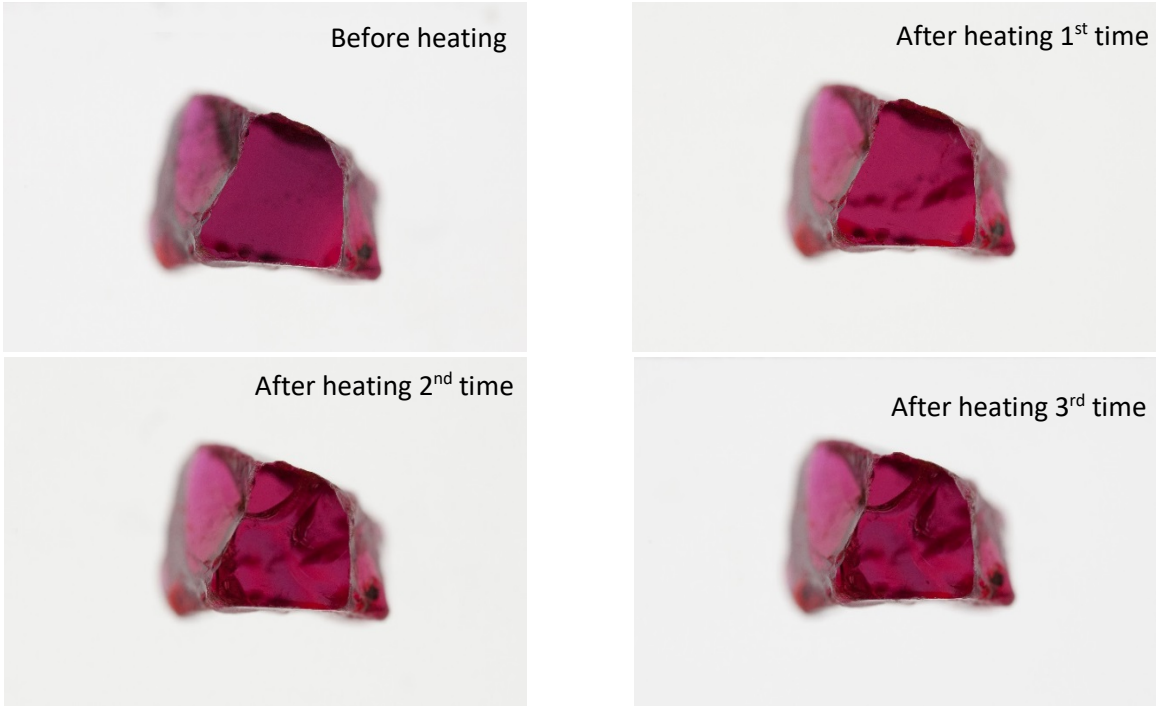

Table A-9: Color-calibrated photo after heat treatment on GIA reference sample #7019 after heating at **800°C for 2 hours and 40 minutes** in air for three consecutive times (thickness 2.608 mm).

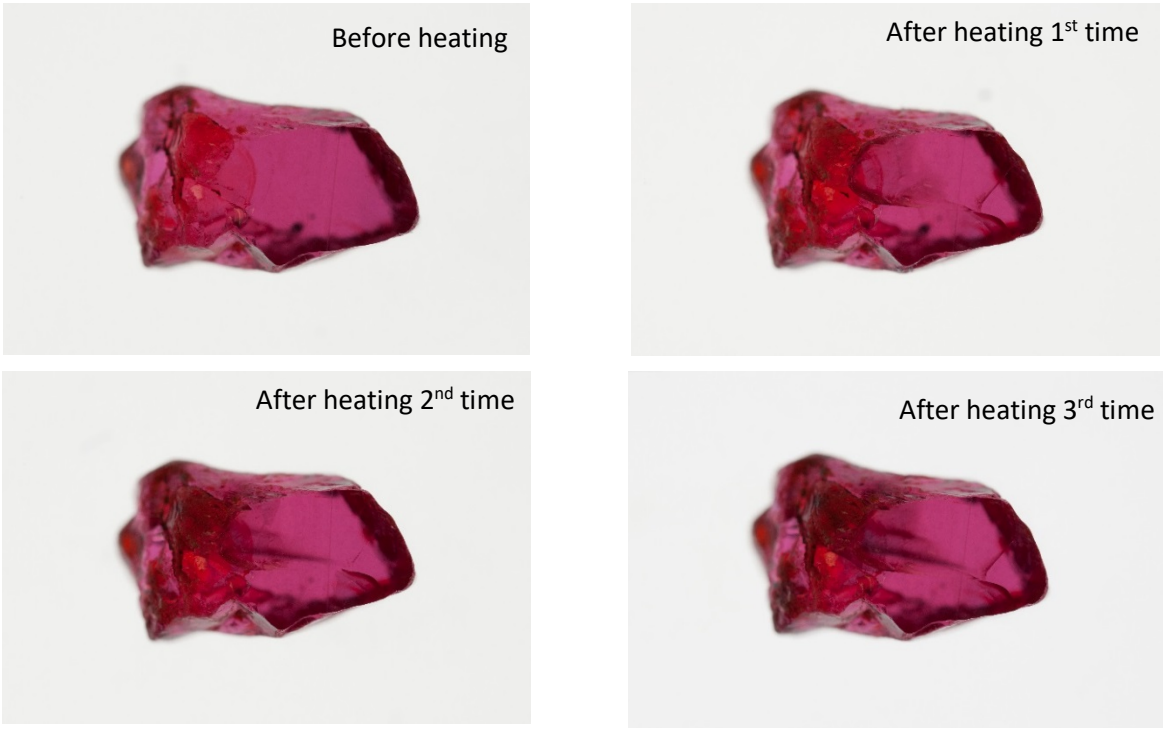

Table A-6: Color-calibrated photo after heat treatment on GIA reference sample #7062 after heating at **800°C for 2 hours and 40 minutes** in air for three consecutive times (thickness 2.514 mm).

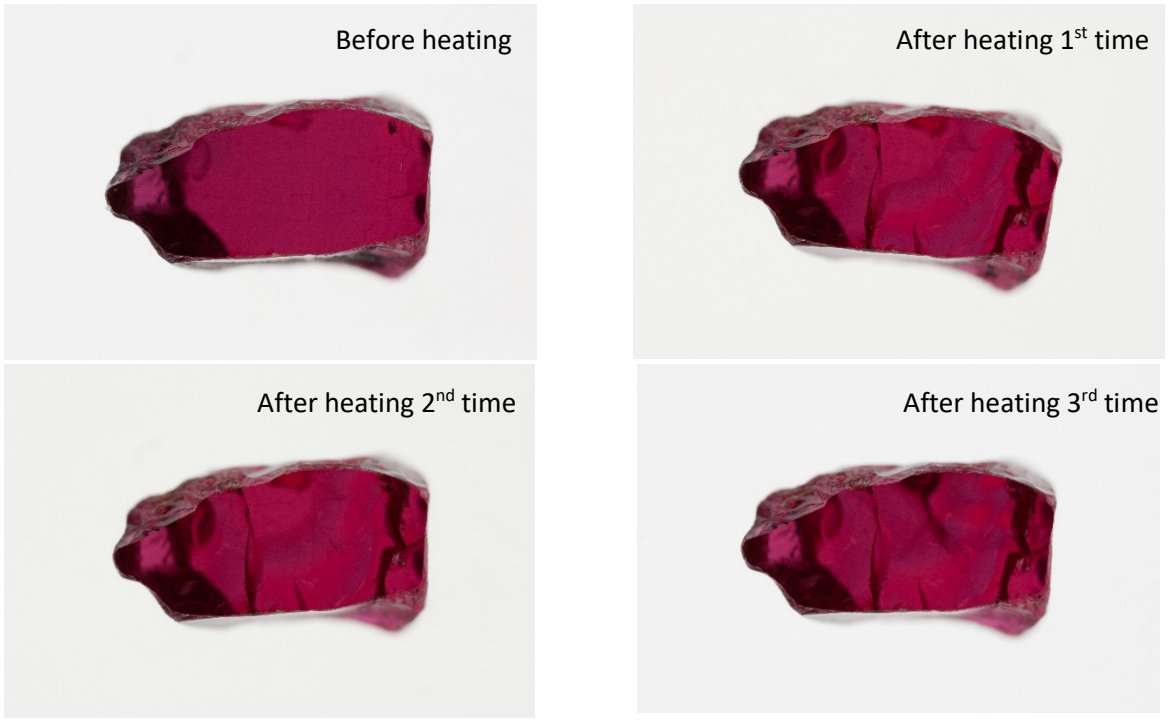

Table A-11: Color-calibrated photo after heat treatment on GIA reference sample #7077 after heating **at 800°C for 2 hours and 40 minutes** in air for three consecutive times (thickness 3.181 mm).

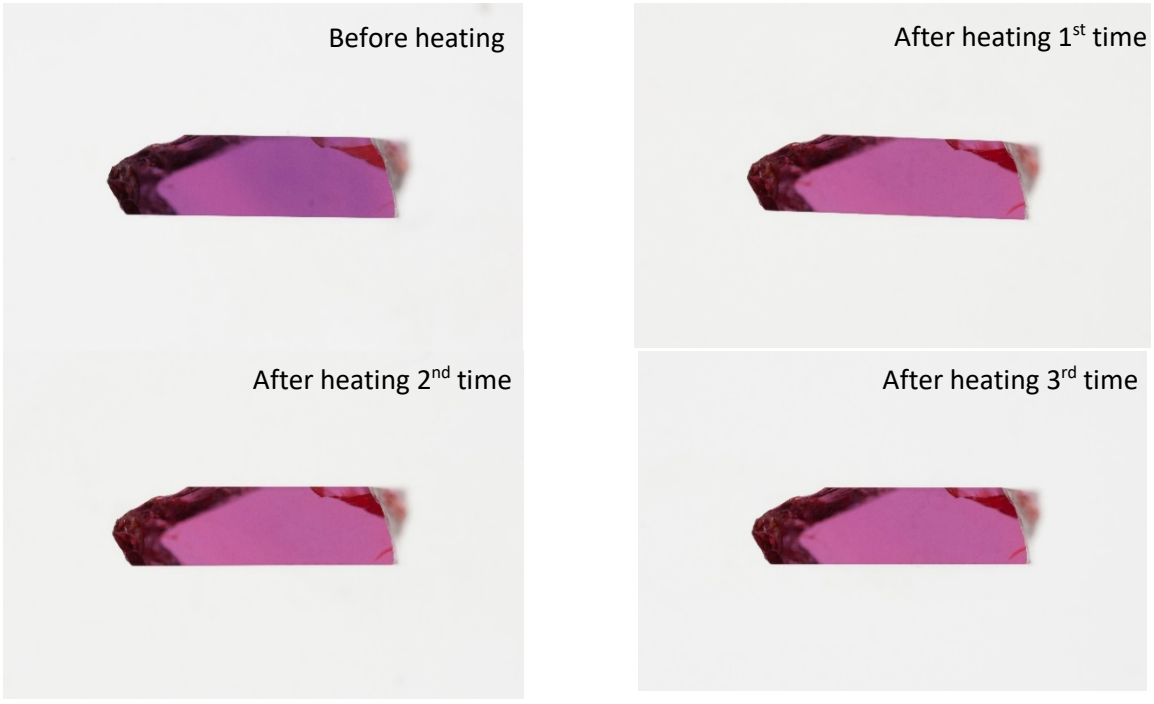

Table A-12: Color-calibrated photo after heat treatment at 800°C for **2 hours and 40 minutes** in air.

No.	Before	After	
0568			Blue color **decreased** after heating Thickness 1.037 mm
0854			**No obvious** change to the blue color Thickness 1.372 mm
0874			Blue color slightly **decreased** after heating Thickness 2.760 mm
0892			**No obvious** change to the blue color Thickness 1.758 mm
0912			Blue color **decreased** after heating Thickness 2.809 mm

No.	Before	After	
0928			**No obvious** change to the blue color Thickness 1.352 mm
0933			**No obvious** change to the blue color Thickness 1.882 mm
0953			**No obvious** change to the blue color Thickness 2.355 mm
0955			Blue color slightly **decreased** after heating Thickness 2.554 mm
0957			Blue color **decreased** after heating Thickness 1.960 mm

No.	Before	After	
6560			Blue color **decreased** after heating Thickness 1.708 mm
6565			Blue color **decreased** after heating Thickness 1.463 mm
7006			Blue color **decreased** after heating Thickness 2.133 mm
7009			Blue color slightly **decreased** after heating Thickness 1.594 mm
7014			**No obvious** change to the blue color Thickness 1.630 mm

No.	Before	After	
7020			Blue color **decreased** after heating Thickness 3.076 mm
7037	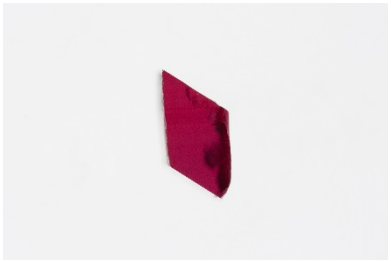	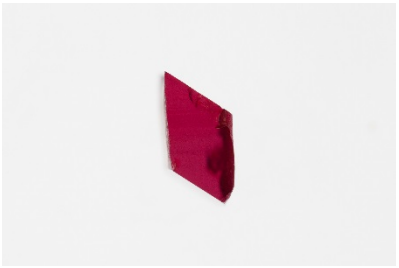	**No obvious** change to the blue color Thickness 3.195 mm
7049			Blue color **decreased** after heating Thickness 2.641 mm
7057			Blue color **decreased** after heating Thickness 1.407 mm
7084			Blue color **decreased** after heating Thickness 1.653 mm